Masterarbeit in Physik

A Two-Potential Formalism For The Pion Vector Form-Factor

von
George Chanturia

angefertigt im
Helmholtz-Institut für Strahlen- und Kernphysik

vorgelegt der
Mathematisch-Naturwissenschaftlichen Fakultät der Universität Bonn

Juli 2021

Ich versichere, dass ich diese Arbeit selbstständig verfasst und keine anderen als die angegebenen Quellen und Hilfsmittel benutzt sowie die Zitate kenntlich gemacht habe.

Bonn, 14.08.2021 . . . .

Datum *Unterschrift*

Gutachter 1: PD Dr. Bastian Kubis

Gutachter 2: Prof. Dr. Christoph Hanhart

Contents

Notation

n_C — number of channels;

n_R — number of resonances;

$(\mathbb{1}_C)_{ij} = \delta_{ij} \quad [i,j = 1,\dots,n_C]$ — identity in "channel space";

$(\mathbb{1}_R)_{ij} = \delta_{ij} \quad [i,j = 1,\dots,n_R]$ — identity in "resonance space";

G_k — propagator of channel k (2.43);

G^l — propagator of resonance l (2.52);

m_l — mass of resonance l (2.52);

g_k^l — coupling between channel k and resonance l (2.51);

c_k — coupling between channel k and external current (2.53);

α^l — coupling between resonance l and external current (2.53);

σ_k — phase space factor for channel k (3.1, 3.5);

ξ_k — centrifugal barrier factor for channel k (3.1, 3.5);

Γ_k — vertex for channel k (C.2);

Σ_k — self-energy for channel k (2.47);

$(\tilde{T})_{kk}$ — elastic T-matrix for channel k (2.42);

$\tilde{\delta}_1$ — phase for $\tilde{t}_{11} \equiv \tilde{t}_1$ (A.7)

$(T_R)_{kj}$ — resonance T-matrix between channels k and j (2.45);

F_k — form factor for channel k (2.49).

Masses and quantum numbers

The values are taken from the [PDG 2020]:

Name	Symbol	Mass	Quantum numbers
Photon	γ	0	$I(J^{PC}) = 0, 1(1^{--})$
Electron	e	511 keV	$J = \frac{1}{2}$
Pion	π	139.57 MeV	$I^G(J^P) = 1^-(0^-)$
Kaon	K	493.67 MeV	$I(J^P) = \frac{1}{2}(0^-)$
Rho	ρ	775.26 MeV	$I^G(J^{PC}) = 1^+(1^{--})$
Omega	ω	782.65 MeV	$I^G(J^{PC}) = 0^-(1^{--})$
Phi	ϕ	1019.46 MeV	$I^G(J^{PC}) = 0^-(1^{--})$

Table 1: Masses and quantum numbers of particles mentioned throughout the text.

1 Motivation

The magnetic moment of the muon g_μ (and the anomalous part

$$a_\mu = \frac{g_\mu - 2}{2},$$

in particular) is one of the most precisely known physical quantities nowadays, both theoretically and experimentally. The most recent Standard Model (SM) prediction reads [Aoyama et al. 2020]

$$a_\mu^{\mathrm{SM}} = 116591810(43) \times 10^{-11}, \tag{1.1}$$

which is smaller than the experimental average of the E821 at Brookhaven [BNL 2006] and E989 at Fermilab [FNAL 2021] by 4.2σ:

$$a_\mu^{\mathrm{Exp.}} = 116592061(41) \times 10^{-11}. \tag{1.2}$$

Because of this discrepancy, a_μ is currently one of the most promising observables to show the need for physics beyond the Standard Model. By convention, the significance of 5σ is needed in order for a claim to be called a discovery. This calls for improvement in precision on both experimental and theoretical sides. Another experiment with a precision goal of 450 parts per billion (similar to the E989 experiment at Fermilab) is planned to run in 2024 [Abe et al. 2019].

This work could help increase the accuracy of the theoretical prediction for the a_μ. The leading contributions from the hadronic sector are the hadronic vacuum polarization (HVP) and the hadronic light-by-light scattering (HLbL) (see Figure 1) with [Aoyama et al. 2020]

$$\begin{aligned} a_\mu^{\mathrm{HVP}} &= 6845(40) \times 10^{-11}, \\ a_\mu^{\mathrm{HLbL}} &= 92(18) \times 10^{-11}. \end{aligned} \tag{1.3}$$

One of the most important contributors to both HVP and HLbL are the two-pion states [Colangelo et al. 2017, 2019]. The coupling of the pions to the electromagnetic current is given by the pion vector form factor (VFF), to be defined later in the text, in Section 2.3.

The pion form factors are most commonly modeled by sums of Breit-Wigners [Gounaris and Sakurai 1968] or the K-matrix formalism [Dalitz 1961]. Since the former violates unitarity and the latter destroys analyticity, a new parametrization is needed, hopefully preserving both of these properties of the S-matrix. In this work we present such a parametrization, using a two-potential formalism, introduced in [Hanhart 2012]. The formalism has been applied to the pion vector form factor in the original paper, to the pion scalar form factor in [Ropertz et al. 2018] and to the scalar pion-kaon form

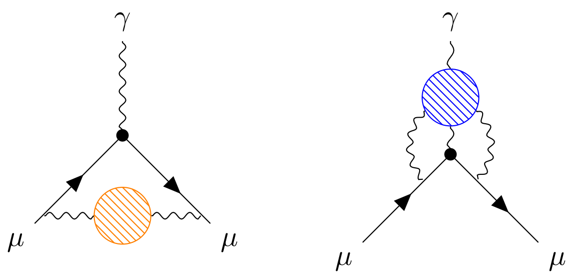

Figure 1: The Hadronic Vacuum Polarization (left) and the Hadronic Light by Light scattering (right) contributions to the anomalous magnetic moment of the muon.

factor in [von Detten et al. 2021]. Here we take a look at the pion vector form factor with exclusive data from the $\pi^0\omega$ channel, which was not included in [Hanhart 2012].

This work is structured as follows. In Section 2 a theoretical introduction is given: scattering kinematics, principles of analyticity and unitarity of the S-matrix, as well as the formal definition of the pion VFF and our approach for its parametrization. Section 3 presents the application of the two-potential formalism to the pion VFF and the results obtained by the fitting procedure. These are followed by Appendices, containing detailed calculations of invariant amplitudes, discontinuity equations, etc.

2 Theory

2.1 Kinematics

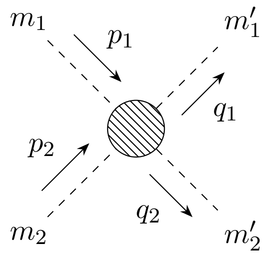

For a $2 \to 2$ process of spinless particles with initial momenta p_1, p_2 and final momenta q_1, q_2, the amplitude can depend only on the scalar products:

$$p_1^2, \quad p_2^2, \quad q_1^2, \quad q_2^2, \quad p_1 \cdot p_2, \quad p_1 \cdot q_1, \quad p_1 \cdot q_2, \quad p_2 \cdot q_1, \quad p_2 \cdot q_2, \quad q_1 \cdot q_2. \tag{2.1}$$

The first 4 are constrained by the mass-shell conditions:

$$p_i^2 = m_i^2, \quad q_i^2 = m_i'^2, \qquad i = 1, 2. \tag{2.2}$$

Energy-momentum conservation gives 4 additional constraints:

$$p_1^\mu + p_2^\mu = q_1^\mu + q_2^\mu, \qquad \mu = 0, 1, 2, 3. \tag{2.3}$$

This fixes 8 out of 10 variables and therefore leaves 2 of them independent. Alternatively to (2.1) one can define three scalar quantities called the Mandelstam variables:

$$\begin{aligned} s &= (p_1 + p_2)^2 = (q_1 + q_2)^2, \\ t &= (p_1 - q_1)^2 = (p_2 - q_2)^2, \\ u &= (p_1 - q_2)^2 = (p_2 - q_1)^2. \end{aligned} \tag{2.4}$$

As discussed above, only two of these variables can be linearly independent. In fact, it can be shown that s, t and u satisfy

$$s + t + u = m_1^2 + m_2^2 + m_1'^2 + m_2'^2. \tag{2.5}$$

The n-particle phase space is defined [PDG 2020] as

$$d\Phi_n = \delta^{(4)} \left(\sum_i p_i - \sum_j q_j \right) \prod_{j=1}^{n} \frac{d^3 q_j}{(2\pi)^3 2E_{\vec{q}_j}}, \tag{2.6}$$

where $E_{\vec{q}_j} = \sqrt{m_j^2 + \vec{q}_j^{\,2}}$. p_i are the initial momenta, while q_j are the final ones.

One could also argue about the near-threshold scaling for the phase space factors by employing simplified dimensional analysis

$$d\Phi_n \sim |\vec{q}_M|^{3n-5}, \tag{2.7}$$

where $|\vec{q}_M|$ is the maximum momentum observed in the final state at given energy $\sqrt{s}$. The power $3n$ comes from the momentum integration measure, while the power of -5 comes from the δ-function (note that even though $\delta^{(4)}$ would in principle introduce 4 powers of momenta in the denominator, energy is proportional to momentum squared near threshold). For example, for a final state of n identical particles with masses m,

$$|\vec{q}_M| \sim \sqrt{1 - \frac{(nm)^2}{s}}. \tag{2.8}$$

The differential cross section for a $2 \to 2$ process is

$$d\sigma_{m_1 m_2 \to m'_1 m'_2} = \frac{(2\pi)^4 \left|\langle q_1, q_2 | t | p_1, p_2\rangle\right|^2}{4\sqrt{(p_1 \cdot p_2)^2 - m_1^2 m_2^2}} d\Phi_2, \tag{2.9}$$

where initial and final states are denoted by $|p_1, p_2\rangle$ and $|q_1, q_2\rangle$, and $m_{1,2}$ are the masses of the particles in the initial state. Of course, they need not to be the same in the final state. We will denote final state masses with $m'_{1,2}$. Using (2.6), we get for a two-body phase space

$$\begin{aligned}
\sigma_{m_1 m_2 \to m'_1 m'_2} &= \int \frac{(2\pi)^4 \delta^{(4)}(p_1 + p_2 - q_1 - q_2)}{4\sqrt{(p_1 \cdot p_2)^2 - m_1^2 m_2^2}} \frac{|t_{fi}|^2}{\mathbb{S}} \frac{d^3 q_1}{(2\pi)^3 2E_{\vec{q}_1}} \frac{d^3 q_2}{(2\pi)^3 2E_{\vec{q}_2}} \\
\xrightarrow{E_{m,\vec{q}_1} = E_{m,-\vec{q}_1} \equiv E_{m,\vec{q}}} &= \frac{1}{16\pi^2 \mathbb{S}} \int \frac{\delta(\sqrt{s} - E_{m'_1,\vec{q}} - E_{m'_2,\vec{q}})}{4\sqrt{(p_1 \cdot p_2)^2 - m_1^2 m_2^2}} \frac{|t_{fi}|^2 \, d^3 q}{E_{m'_1,\vec{q}} E_{m'_2,\vec{q}}} \\
&= \frac{1}{16\pi^2 \mathbb{S}} \frac{\sqrt{\lambda(s, m_1'^2, m_2'^2)}}{2s} \frac{1}{4\sqrt{(p_1 \cdot p_2)^2 - m_1^2 m_2^2}} \int |t_{fi}|^2 \, d\Omega_{\vec{q}},
\end{aligned} \tag{2.10}$$

where $\mathbb{S}$ is the symmetry factor and λ is the Källén function, defined as

$$\lambda\left(s, m_1^2, m_2^2\right) = \left(s - (m_1 + m_2)^2\right)\left(s - (m_1 - m_2)^2\right). \tag{2.11}$$

In the CM frame, where $\vec{p}_1 = -\vec{p}_2 \equiv \vec{p}$, the Källén function gives the solution of

$$\begin{aligned}
&\sqrt{s} = \sqrt{m_1 + \vec{p}^{\,2}} + \sqrt{m_2 + \vec{p}^{\,2}}, \\
\implies \quad &\vec{p}^{\,2} = \frac{\lambda(s, m_1^2, m_2^2)}{4s} = \frac{\left(s - (m_1 + m_2)^2\right)\left(s - (m_1 - m_2)^2\right)}{4s}.
\end{aligned} \tag{2.12}$$

The flux factor in the denominator of (2.10) is given by

$$4\sqrt{(p_1 \cdot p_2)^2 - m_1^2 m_2^2} = 4\sqrt{s}|\vec{p}| = 2\sqrt{\lambda(s, m_1^2, m_2^2)}. \tag{2.13}$$

Therefore,

$$\sigma_{m_1 m_2 \to m'_1 m'_2} = \frac{1}{64\pi^2} \frac{\sqrt{\lambda(s, m_1'^2, m_2'^2)}}{\sqrt{\lambda(s, m_1^2, m_2^2)}} \frac{1}{s} \int \frac{|t_{fi}|^2}{\mathbb{S}} d\Omega_{\vec{q}}. \tag{2.14}$$

2.2 Properties of the S-matrix

2.2.1 Analyticity

The S-matrix, as a function on the complex E plane, is assumed to be analytic up to branch points and poles, so that the theory is causal [Eden et al. 1966]. These are the continuous right-hand cuts from threshold to ∞ (associated with allowed intermediate states) and discrete poles at negative real values of E (associated with bound states).

This allows us to write a dispersion relation by employing Cauchy's theorem. We start by choosing a contour that avoids all the possible poles, as displayed on Figure 3. We also assume that $S(E)$ falls sufficiently fast for large E, so that large arcs do not contribute.

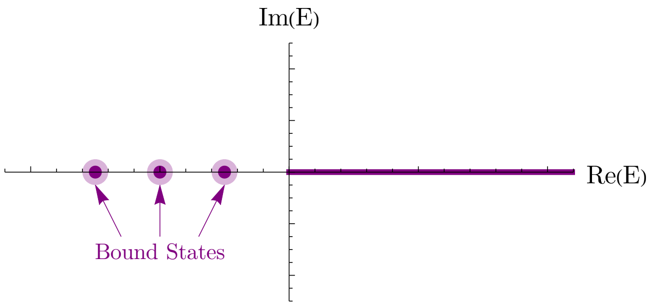

Figure 2: General analytic structure of the S-matrix.

Then, $S(E)$ is analytic in the region enclosed by the path and we get

$$\begin{aligned} S(E) &= \frac{1}{2\pi i}\oint \frac{S(E')dE}{E'-E} \\ \xrightarrow{\text{3 contributions:}} &= \underbrace{\frac{1}{2\pi i}\int_0^\infty \frac{S(E'+i\epsilon)dE}{E'-E}}_{\text{Above}} + \underbrace{\frac{1}{2\pi i}\int_\infty^0 \frac{S(E'-i\epsilon)dE}{E'-E}}_{\text{Below}} - \underbrace{\sum_j \frac{1}{2\pi i}\oint_{C_j} \frac{S(E')dE}{E'-E}}_{\text{Around the poles}}. \end{aligned} \tag{2.15}$$

The contribution from the large arcs are ignored and the minus sign in front of the last term accounts for a reversed direction when integrating around the poles. The loops around the poles can be made small enough, such that they enclose a single pole only. Thus, we may write for a given j:

$$\frac{1}{2\pi i}\oint_{C_j} \frac{S(E')dE}{E'-E} = \frac{1}{2\pi i}\oint_{C_j} \frac{\mathrm{Res}_{E_j}(S)}{(E'-E_j)(E_j-E)} = -\frac{\mathrm{Res}_{E_j}(S)}{E-E_j}. \tag{2.16}$$

Using the Schwarz reflection principle,

$$\frac{1}{2\pi i}\int_\infty^0 \frac{S(E'-i\epsilon)}{E'-E}dE' = \frac{-1}{2\pi i}\int_0^\infty \frac{S(E'+i\epsilon)^*}{E'-E}dE'. \tag{2.17}$$

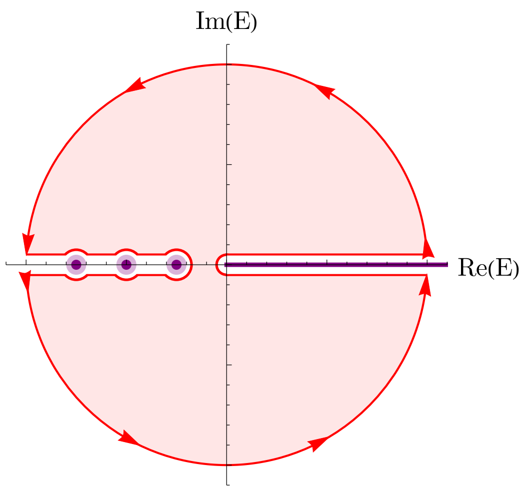

Figure 3: Integration contour on the complex E-plane.

With $S(E'+i\epsilon) - S(E'+i\epsilon)^* = 2i\mathrm{Im}(S(E'))$ one finds

$$S(E) = \frac{1}{\pi}\int_0^\infty \frac{\mathrm{Im}(S(E'))}{E'-E} dE' + \sum_j \frac{\mathrm{Res}_{E_j}(S)}{E-E_j}. \tag{2.18}$$

This relation is trivially correct for the imaginary part on the real axis of the physical sheet. For values at $E+i\epsilon$ we use the following relation

$$\frac{1}{x-x_0-i\epsilon} \xrightarrow{\epsilon\to 0} \frac{\mathcal{P}}{x-x_0} + i\pi\delta(x-x_0), \tag{2.19}$$

where $\mathcal{P}$ denotes the principal value. Hence,

$$\begin{aligned} S(E+i\epsilon) &= \frac{1}{\pi}\,\mathcal{P}\!\!\int_0^\infty \frac{\mathrm{Im}(S(E'))}{E'-E} dE' + i\mathrm{Im}(S(E+i\epsilon)) + \sum_j \text{Poles} \\ \implies \mathrm{Re}(S(E+i\epsilon)) &= \frac{1}{\pi}\,\mathcal{P}\!\!\int_0^\infty \frac{\mathrm{Im}(S(E'))}{E'-E} dE' + \sum_j \text{Poles}. \end{aligned} \tag{2.20}$$

By assumption, $S(E)$ is (analytic and thus) infinitely differentiable:

$$S(E) = S(E_0) + S'(E_0)(E-E_0) + \dots \tag{2.21}$$

So, instead of $S(E)$, one can write dispersion relations for

$$S_1(E) = \frac{S(E)-S(E_0)}{E-E_0}. \tag{2.22}$$

Note that $S_1(E)$ is regular at $E=E_0$ and drops faster than $S(E)$ by one power in E:

$$S_1(E) = \frac{1}{\pi}\int_0^\infty \frac{\mathrm{Im}(S_1(E'))}{E'-E} dE' + \text{Bound states}, \tag{2.23}$$

or, using the definition of $S_1(E)$,

$$S(E) = S(E_0) + \frac{E-E_0}{\pi}\int_0^\infty \frac{\mathrm{Im}(S(E'))}{(E'-E)(E'-E_0)}. \tag{2.24}$$

$S(E_0)$ here is called a subtraction constant. This procedure may be repeated to introduce further subtraction constants. For instance, the next step would be

$$S_2(E) = \frac{S(E)-S(E_0)-S'(E_0)(E-E_0)}{(E-E_0)^2}. \tag{2.25}$$

This introduces another subtraction constant $S'(E_0)$ and adds another negative power of E into the integrand. Therefore, we can always force the integral to converge. If this is done n times, we have n subtractions constants: $S(E_0), S'(E_0), \dots, S^{(n)}(E_0)$. The n-times subtracted dispersion integral reads

$$\begin{aligned} S(E) = S(E_0) + S'(E_0)(E-E_0) + \dots + \frac{1}{(n-1)!}S^{(n-1)}(E_0)(E-E_0)^{n-1} + \\ + \frac{(E-E_0)^n}{\pi}\int_0^\infty \frac{\mathrm{Im}(S(E'))}{(E'-E_0)^n(E'-E)}. \end{aligned} \tag{2.26}$$

2.2.2 Unitarity

Due to probability conservation, the S-matrix is required to be unitary [PDG 2020]: $S^\dagger S = SS^\dagger = \mathbb{1}$. We define the T-matrix as:

$$\begin{aligned} S &= \mathbb{1} - iT, \\ \langle f|T|i\rangle &= (2\pi)^4\delta^{(4)}(P_f - P_i)t_{fi}, \end{aligned} \tag{2.27}$$

where P_i and P_f are the total 4-momenta of states $|i\rangle$ and $|f\rangle$, respectively.

The unitarity relation for S implies that $T - T^\dagger = -iTT^\dagger$. Using (2.27), we can write

$$\begin{aligned} \langle f|T - T^\dagger|i\rangle &= -i\,\langle f|T^\dagger T|i\rangle\,, \\ (2\pi)^4\delta^{(4)}(P_f - P_i)\left(t_{fi} - t_{if}^*\right) &= -i\sum_n (2\pi)^4\delta^{(4)}(P_f - P_n)(2\pi)^4\delta^{(4)}(P_n - P_i)t_{nf}^* t_{ni}, \\ \implies \quad t_{fi} - t_{if}^* &= -i\sum_n (2\pi)^4\delta^{(4)}(P_f - P_n)t_{nf}^* t_{ni}. \end{aligned} \tag{2.28}$$

This can be used to determine discontinuities due to the allowed intermediate states. Examples are given in the following sections.

2.3 Definition of the form factor

The central object of interest throughout this work is the pion vector form factor $F_V(s)$ defined as

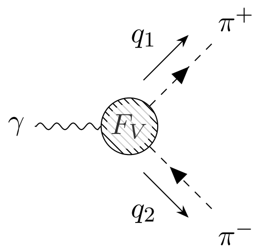

$$= \langle \pi^+(q_1)\pi^-(q_2)|J^\mu|0\rangle = e(q_1 - q_2)^\mu F_V(s), \tag{2.29}$$

where s is the Mandelstam variable $s = (q_1 + q_2)^2$. This object can be extracted e.g. from the process $e^+e^- \to \pi^+\pi^-$, where one has to contract the hadronic current given in (2.29) and the photon propagator with the leptonic current, which is defined as

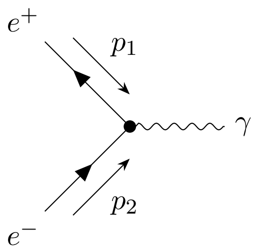

$$= \langle 0|J^\mu|e^+(p_1)e^-(p_2)\rangle = \bar{v}(p_1)\left(-ie\gamma^\mu\right)u(p_2). \tag{2.30}$$

(See Appendix B for a detailed calculation.)

2.4 Elastic regime

The discontinuity of $F_V(s)$ comes from the allowed intermediate states. For energies below the first inelastic threshold, the only intermediate state (reachable through strong interactions) is the two-pion elastic channel (see Figure 4).

The corresponding discontinuity is (see the derivation of (A.13))

$$\mathrm{disc}\,[F_V(s)] = 2i\sigma(s)\tilde{t}_1^*(s)F_V(s), \tag{2.31}$$

where

$$\sigma(s) = \frac{1}{16\pi}\sqrt{1-\frac{4m_\pi^2}{s}} \tag{2.32}$$

and $\tilde{t}_1(s)$ is the P-wave projection of the elastic scattering t-matrix, which can be parametrized as

$$\tilde{t}_1(s) = \frac{1}{\sigma(s)}\sin(\tilde{\delta}(s))e^{i\tilde{\delta}(s)}. \tag{2.33}$$

Using (2.31, 2.33), one obtains Watson's theorem [Watson 1954]:

$$\begin{aligned}&\left(\mathrm{Im}[F_V(s)] = \sin(\tilde{\delta}_1(s))e^{-i\tilde{\delta}_1(s)}F_V(s)\right) \in \mathbb{R}\\ \implies\ &\arg[F_V(s)] = \tilde{\delta}_1(s).\end{aligned} \tag{2.34}$$

Once $\tilde{\delta}_1$ is known, we may construct F_V from this. Assume Ω is a solution of the discontinuity equation. Then $F_V(s) = P(s)\Omega(s)$ is a solution as well, provided that $P(s)$ is free of right-hand cuts and poles up to inelastic thresholds and can be approximated as a polynomial at low energies.

We may solve Ω under the assumption that it does not have any zeros and $\Omega(0) = 1$.

$$\begin{aligned}&\Omega(s+i\varepsilon) = |\Omega(s)|e^{i\tilde{\delta}_1(s)}\\ \implies\ &\Omega(s-i\varepsilon) = \Omega(s+i\varepsilon)^* = |\Omega(s)|e^{-i\tilde{\delta}_1(s)}\\ &\qquad\qquad\quad = \Omega(s+i\varepsilon)e^{-2i\tilde{\delta}_1(s)}.\end{aligned} \tag{2.35}$$

Since $\Omega(s)$ does not have any zeros, we can take the logarithm:

$$\begin{aligned}&\ln(\Omega(s-i\varepsilon)) = \ln(\Omega(s+i\varepsilon)) - 2i\tilde{\delta}_1(s),\\ \implies\ &\mathrm{disc}(\ln(\Omega(s))) = 2i\tilde{\delta}_1(s).\end{aligned} \tag{2.36}$$

Assume $\delta(s\to\infty)\to$ const.; then one can write a once-subtracted dispersion integral for $\ln(\Omega)$:

$$\ln(\Omega(s)) = \underbrace{\ln(\Omega(0))}_{=0} + \frac{s}{\pi}\int_{s_{\mathrm{thr}}}^{\infty}\frac{\tilde{\delta}_1(s')ds'}{s'(s'-s)}. \tag{2.37}$$

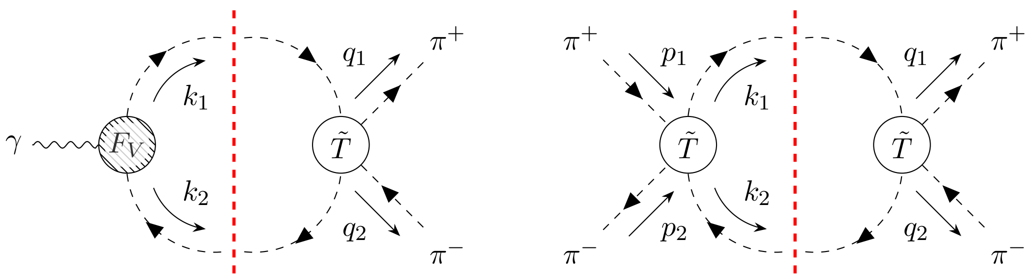

Figure 4: Cutkosky cuts due to the 2π elastic channel for the form factor (left) and the transition matrix element (right).

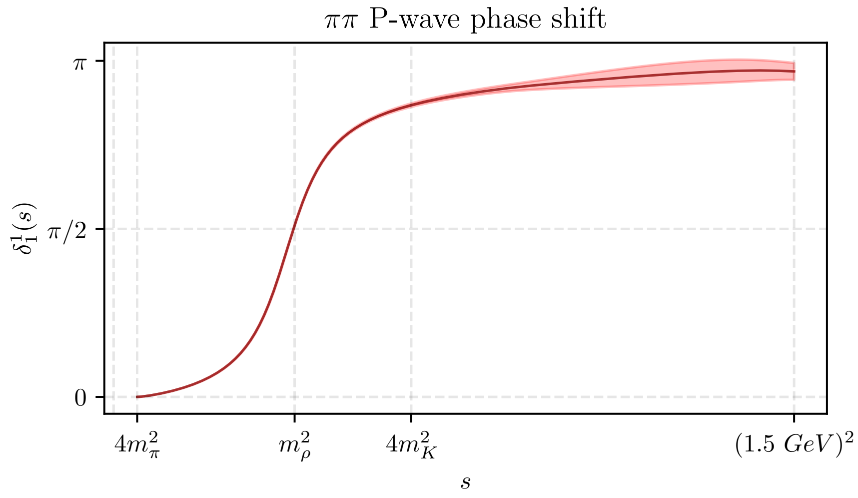

Figure 5: The pion P-wave phase shift [Colangelo et al. 2019].

Finally [Omnès 1958],

$$\Omega(s) = \exp\left(\frac{s}{\pi}\int_{s_{\text{thr}}}^{\infty}\frac{\tilde{\delta}_1(s')ds'}{s'(s'-s-i\varepsilon)}\right). \tag{2.38}$$

For the input phase $\tilde{\delta}_1$ we use $\pi\pi$ P-wave phase shifts from [Colangelo et al. 2001, 2019], plotted in Figure 5. They are valid up to $s = (1.5\text{ GeV})^2$. From that point on we smoothly guide it to the value of π using

$$\tilde{\delta}_1(s) = \pi + \left(\tilde{\delta}\left((1.5\text{ GeV})^2\right) - \pi\right)\left(\frac{\lambda^2 + (1.5\text{ GeV})^2}{\lambda^2 + s}\right) \qquad [\text{for } s > (1.5\text{ GeV})^2]. \tag{2.39}$$

(2.39) introduces a pole in the spacelike region: $s = -\lambda^2$. However, provided λ is sufficiently large, this does not have visible consequences on the amplitude in the timelike region. We take $\lambda = 10$ GeV. The comparison of the Omnès solution to the pion vector form factor data [BaBaR 2012] is given in Figure 6.

One can notice that the Omnès function, although it gives a decent description of the data at low energies, deviates largely from the experimental values above 1 GeV or so. Apart from that, it fails to account for the isospin-breaking effects such as $\rho - \omega$ and $\rho - \phi$ mixing, depicted on the upper panels of Figure 6.

The data show pronounced structures above 1 GeV, which could be described by introducing resonances. These resonances, however, do not show up in the $\pi\pi$ scattering phase (see Figure 5). This could be resolved by introducing inelastic channels. Then, Watson's theorem (2.34) does not hold anymore and the scattering phase does not necessarily agree with the phase of the form factor. So, the phase motion due to the higher resonances can appear in the form factor only.

2.5 Including inelastic channels: two-potential formalism

Following the discussion in the previous section, a formalism is required that (a) maps smoothly onto the Omnès solution at low energies and (b) fits the data well at higher energies. We have already argued that in addition to the elastic channel, the model should contain contributions from inelastic ones.

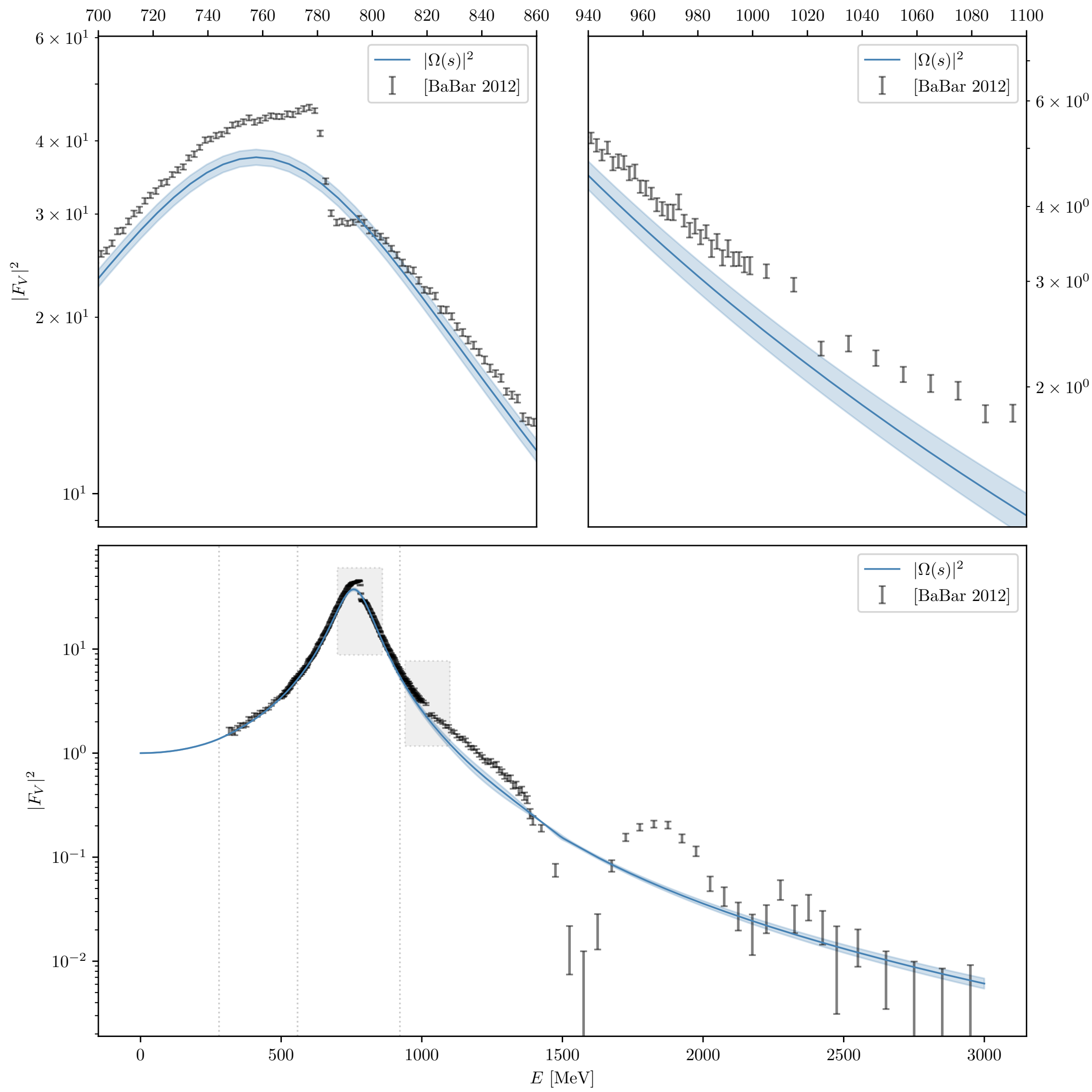

Figure 6: The Omnès solution compared to the experimental data for $F_V(s)$ from [BaBaR 2012]. The input phase shift $\tilde{\delta}(s)$ is from [Caprini et al. 2012], extrapolated to π using (2.39). The upper panels show the effects of $\rho - \omega$ (left) and $\rho - \phi$ (right) mixing in the data. The dotted lines denote thresholds for the $\pi\pi$, 4π and $\pi^0\omega$ channels.

We denote the interaction potential between channels i and j with $V_{ij}(s)$ and split it into two parts:

$$V_{ij}(s) = \tilde{V}_{ij}(s) + V_{Rij}(s), \tag{2.40}$$

where $\tilde{V}$ describes elastic interaction. Such a splitting, applied to the pion vector form factor, was introduced in [Hanhart 2012], inspired by e.g. [Nakano 1982]. The subscript R in V_R indicates that the inelastic part of the potential will be attributed to resonances. The explicit expression for V_R within this model will be given below. We will also see that there is no need to specify the explicit form of the elastic potential $\tilde{V}$, all we need are the phase shifts.

Accordingly, the scattering matrix can be split into an elastic part and a remainder:

$$T_{ij}(s) = \tilde{T}_{ij}(s) + T_{Rij}(s). \tag{2.41}$$

The elastic part of the T-matrix is, of course, diagonal in i, j and can be obtained from $\tilde{V}$ using the

Lippmann-Schwinger equation:

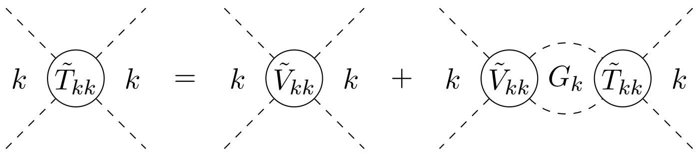

$$\Longrightarrow \quad \tilde{T} = \tilde{V} + \tilde{V} G \tilde{T} \tag{2.42}$$

Here G_k denotes the propagation of channel k. For instance, in the case of the 2π channel ($k = 1$), we have

$$G_1 = \int \frac{d^4 l}{(2\pi)^4} \, |l, P-l\rangle \, \frac{1}{(l^2 - m_\pi^2 + i\epsilon)} \frac{1}{((P-l)^2 - m_\pi^2 + i\epsilon)} \, \langle l, P-l| \,, \tag{2.43}$$

where $P^2 = s$. With this we define "in" and "out" vertices to be

$$\Gamma_{\text{in}}^\dagger = 1 + G\tilde{T}, \qquad \Gamma_{\text{out}} = 1 + \tilde{T}G. \tag{2.44}$$

Since only *elastic* scattering is included in the definition of the vertex, its discontinuity equation is the same as of the Omnès function (2.38). Therefore, the vertex of the first channel will be taken to be $\Gamma_1 = \Omega[\tilde{\delta}]$. The parametrization of the other vertices is discussed in Section 3.1.

To obtain T_R from the resonance potential, we first split it as

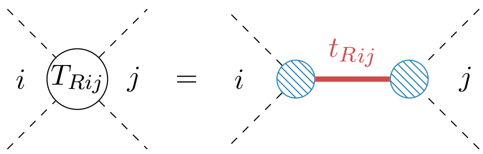

$$\Longrightarrow \quad T_{Rij} = \xi_i \Gamma_{\text{out},i} t_{Rij} \Gamma_{\text{in},j}^\dagger \xi_j. \tag{2.45}$$

Along with the vertices Γ_i we have also pulled out the centrifugal barrier factors ξ_i. These are the factors that come from the Lorentz structure that the form factors are multiplied with (see (2.29) and Appendix B for details). Explicit functional forms for ξ_i will be discussed in section 3.1. t_{Rij} is then defined as

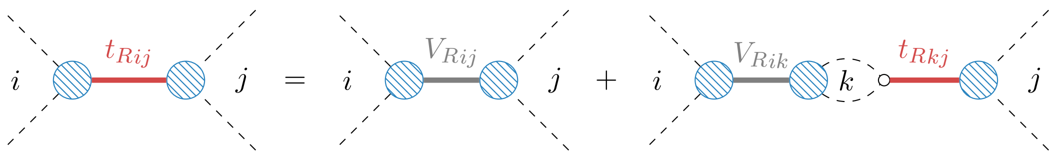

$$\begin{aligned} t_{Rij} &= V_{Rij} + V_{Rik} \underbrace{\xi_k G_k \Gamma_k \xi_k}_{\Sigma_k} t_{Rkj}, \\ \Longrightarrow \quad t_R &= \left[\mathbb{1}_C - V_R \Sigma\right]^{-1} V_R. \end{aligned} \tag{2.46}$$

For a detailed calculation see Appendix C.1. The self-energy Σ_k can be calculated using its discontinuity (see the derivation leading to (C.4)):

$$\Sigma_k(s) = \frac{s}{\pi} \int_{s_{\text{thr},k}}^\infty \frac{ds'}{s'} \frac{\sigma_k(s') \xi_k^2(s') |\Gamma_k(s')|^2}{s' - s - i\epsilon}. \tag{2.47}$$

We proceed with the definition of the form factor. We denote point-like source terms for channel k with M_k. Since there are multiple channels open, one needs to allow for inelastic scattering in the full expression. So,

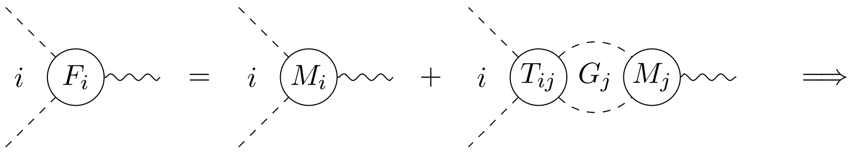

$$\xi_i F_i = \xi_i M_i + T_{ij} G_j \xi_j M_j. \tag{2.48}$$

As already discussed above, the inclusion of the centrifugal barrier factors is needed. Using the definition of T_{ij} along with (2.48), one obtains (see the full derivation in Appendix C.2)

$$F_i = \Gamma_{\text{out},i} [\mathbb{1}_C - V_R \Sigma]^{-1}_{ij} M_j. \tag{2.49}$$

Since this expression was derived from unitarity (we have thoroughly followed the dispersion relations), F_i defined in (2.49) satisfies the expected discontinuity equation (see (C.13) in Appendix C.2):

$$\text{disc}\,[F_i] = 2i T^*_{ik} \sigma_k (\xi_k/\xi_i) F_k, \tag{2.50}$$

as long as the model parameters are real.

2.5.1 The resonance model

To proceed, we need to introduce some model-dependent assumptions: $\tilde{V}_{ij}$ is only non-zero for $i = j = 1$ (a generalization of this for the case of two input channels can be found in [Ropertz et al. 2018]). This means that the elastic scattering matrix, in addition to being diagonal, is zero for every channel other than the first one. All long-ranged forces of the first channel that induce the left-hand cuts are contained in $\tilde{V}$, while no left-hand cuts are allowed in the other channels. All the deviations from $\tilde{V}$ are assumed to come either from s-channel resonances or contact terms. With this [Hanhart 2012], V_R can be defined as

$$\bar{V}_{Rij}(s) = -\sum_{l,l'}^{n_R} g_i^{(l)} G^{(l,l')}(s) g_j^{(l')}, \quad V_{Rij}(s) = \bar{V}_{Rij}(s) - \bar{V}_{Rij}(0), \tag{2.51}$$

where

$$G^{(l,l')}(s) = \frac{\delta_{l,l'}}{s - m_l^2}. \tag{2.52}$$

Here n_R is the number of resonances in the model, $g_i^{(l)}$ denotes the coupling of channel i with resonance l and $G^{(l,l')}$ is the resonance propagator. Even though the bare propagator is diagonal, after photon mixing is taken into account, this is no longer the case (see (2.55) below). m_l is the bare mass of the resonance l. We have subtracted the potential at $s = 0$, so that it does not distort the low-energy region, where the dominant contribution needs to be from $\tilde{V}$.

For the point-like source term M_k we write

$$M_k(s) = c_k - \sum_{l,l'}^{n_R} g_k^{(l)} G^{(l,l')} \alpha^{(l')} s. \tag{2.53}$$

The parameters c_k and $\alpha^{(l)}$ denote the photon coupling with channel k and resonance l, respectively. Resonances couple to the photon linearly in s. This means that the interaction is given via $F^{\mu\nu}V_{\mu\nu}$, where $F_{\mu\nu}$ and $V^{\mu\nu}$ are the field strength tensors for the electromagnetic and the resonance fields, respectively. This kind of coupling ensures gauge invariance.

The couplings $g_i^{(l)}, c_k, \alpha^{(l)}$ and the resonance masses m_l will be treated as the parameters of the fit. The c_k denote the values of F_k at $s = 0$. Therefore, c_1 is fixed to 1 with $F_1(0) = 1$ due to the charge of the pion.

2.5.2 $\rho - \omega$ and $\rho - \phi$ mixing

As already mentioned, we have the effects of ρ mixing with ω and ϕ, depicted on the upper panels of Figure 6. This can be included in the model using

$$c_1 \to c_1 \left(1 + \kappa_\omega \frac{s}{s - m_\omega^2 + i m_\omega \Gamma_\omega} + \kappa_\phi \frac{s}{s - m_\phi^2 + i m_\phi \Gamma_\phi}\right), \tag{2.54}$$

where $\kappa_{\omega/\phi}$ are two additional free parameters of the model, which parametrize the strength of $\rho - \omega/\phi$ mixing. The values for $m_{\omega,\phi}$ and $\Gamma_{\omega,\phi}$ are taken from [PDG 2020]. Note that this redefinition destroys unitarity: M_k now acquires an imaginary part, which was assumed to be absent in the derivation of (C.13) in Appendix C.2. However, since they violate isospin, these effects must be small (as demonstrated in Figure 6). In principle, it is possible to resolve this breaking of unitarity by including additional channels, reached by isospin-breaking reactions. This, in turn, adds free parameters and further complicates the fitting procedure. So, instead, the above strategy was chosen within the scope of this work.

2.5.3 Photon-resonance mixing

One of the well-established effects is the mixing of a ρ with a photon [Jegerlehner and Szafron 2011]. In our framework we can also allow for photon mixing with higher resonances. For this, one needs to redefine the propagator and the vertex as follows:

$$\begin{aligned} G^{(l,l')} \to \hat{G}^{(l,l')} &\equiv G^{(l,l')} + \sum_{l_1,l_2}^{n_R} G^{(l,l_1)} \left(\alpha^{(l_1)} s\right) \frac{1}{s} \left(\alpha^{(l_2)} s\right) G^{(l_2,l')} + \dots \\ \implies G \to \hat{G} &\equiv \left[\mathbb{1}_R - G s \alpha \alpha^T\right]^{-1} G, \end{aligned} \tag{2.55}$$

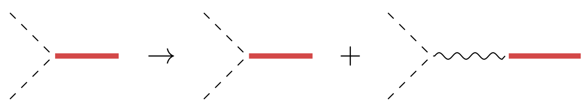

$$g_i^{(l)} \to \hat{g}_i^{(l)} \equiv g_i^{(l)} - e^2 \alpha^{(l)} c_i. \tag{2.56}$$

Finally, we rewrite the potential

$$\bar{V}_{Rij}(s) = -\sum_{l,l'}^{n_R} \hat{g}_i^{(l)} \hat{G}^{(l,l')} \hat{g}_j^{(l')}, \qquad V_{Rij}(s) = \bar{V}_{Rij}(s) - \bar{V}_{Rij}(0) - e^2 \frac{c_i c_j}{s}, \tag{2.57}$$

and the source term

$$M_k(s) = c_k - \sum_{l,l'}^{n_R} \hat{g}_k^{(l)} \hat{G}^{(l,l')} \alpha^{(l')} s. \tag{2.58}$$

Consequently, photon mixing does not introduce new parameters. This was expected, since the parameters for the photon coupling with both the continuum channels and the resonances were already defined.

Note, that the potential is non-zero at $s = 0$ now. Consequently, to retain the previous normalization, one needs to redefine c_i as follows (see Appendix C.2.1 for details):

$$c_i \to c_i \left(1 + \frac{e^2}{\pi} \sum_k c_k^2 \int_{s_{\mathrm{thr},i}}^{\infty} \frac{ds' \sigma_k(s') \xi_k^2(s') |\Gamma_k(s')|^2}{(s')^2}\right). \tag{2.59}$$

2.5.4 Fitting parameters

The model defined as above has the following parameters:

$$\begin{aligned} m_l &- \; n_R \text{ resonance masses;} \\ g_i^{(l)} &- \; n_C \times n_R \text{ channel-resonance couplings;} \\ \alpha^{(l)} &- \; n_R \text{ resonance-photon couplings;} \\ c_k &- \; n_C - 1 \text{ channel-photon couplings;} \\ \kappa_{\omega/\phi} &- \; 2 \text{ strength parameters for } \omega/\phi \text{ mixing.} \end{aligned}$$

where n_C is the number of channels. For instance, the model with $n_C = 3$ channels and $n_R = 2$ resonances would have 14 parameters to be determined by fitting to data. Note that $c_1 = 1$ is fixed by charge conservation, so only $c_2, \ldots, c_{n_C}$ can be adjusted by the fit. In principle, other c_i could also be fixed (see e.g. equation (5.11) in [Schneider 2012] which can be used to fix c_3). In this work, however, only c_1 is fixed.

3 Application

3.1 Channels

The pion vector form factor is related to $\pi\pi$ scattering in P-wave. Therefore, we will consider channels with $I = 1, L = 1$. For the special case of 2-particle final states with masses m_a and m_b, the phase space and the centrifugal barrier factors are

$$\begin{aligned} \sigma_{ab}(s) &= \frac{\sqrt{\lambda(s, m_a^2, m_b^2)}}{s} \frac{1}{16\pi} \quad \text{and} \\ \xi_{ab}(s) &= \frac{\sqrt{\lambda(s, m_a^2, m_b^2)}}{\sqrt{3s}}. \end{aligned} \tag{3.1}$$

The factors of $\sqrt{3}$ appear due to the P-wave projection (see Appendix B for details). We are going to look at the cross sections of e^+e^- going to some channel i, defined as

$$\sigma_{e^+e^- \to i} = \underbrace{(4\pi)^2\alpha^2}_{e^4} \frac{1}{s^2} \sigma_i(s) \left[\xi_i(s)\right]^2 |F_i(s)|^2 . \tag{3.2}$$

The first to consider is the 2π channel, with

$$\begin{aligned} E_{\text{thr},1} &= 2m_\pi \approx 279 \text{ MeV}, \\ \sigma_1(s) &= \frac{1}{16\pi}\sqrt{1 - \frac{4m_\pi^2}{s}}, \\ \xi_1(s) &= \frac{1}{\sqrt{3}}\sqrt{s - 4m_\pi^2}, \\ \Gamma_1(s) &= \Omega[\tilde{\delta}](s). \end{aligned} \tag{3.3}$$

One can check that plugging the above expressions into (3.2) yields

$$\sigma_{e^+e^- \to \pi^+\pi^-} = \frac{\pi\alpha^2}{3} \frac{\lambda^{3/2}(s, m_\pi^2, m_\pi^2)}{s^4} |F_1(s)|^2 \tag{3.4}$$

The second channel contains 4 pions:

$$\begin{aligned} E_{\text{thr},2} &= 4m_\pi \approx 558 \text{ MeV}, \\ \sigma_2(s) &= \frac{1}{16\pi}\sqrt{1 - \frac{16m_\pi^2}{s}}^{\,7}, \\ \xi_2(s) &= \frac{1}{\sqrt{3}}\sqrt{s - 16m_\pi^2}, \\ \Gamma_2(s) &= \frac{\Lambda^2}{\Lambda^2 + s}. \end{aligned} \tag{3.5}$$

For the phase space and centrifugal barrier factors we have used (2.7, 2.8). Unlike the $\pi\pi$ channel, we do not have an input vertex. Instead, we use (3.5), which goes as $\sim 1/s$ for high energies and has a pole in the spacelike region. However, provided that Λ^2 is large enough, this should not affect the timelike region significantly. Therefore, we do not expect the results to be sensitive to the actual value of Λ, which will not be fixed by the fitting procedure. Instead, we will manually vary it over some range, to estimate systematic uncertainties.

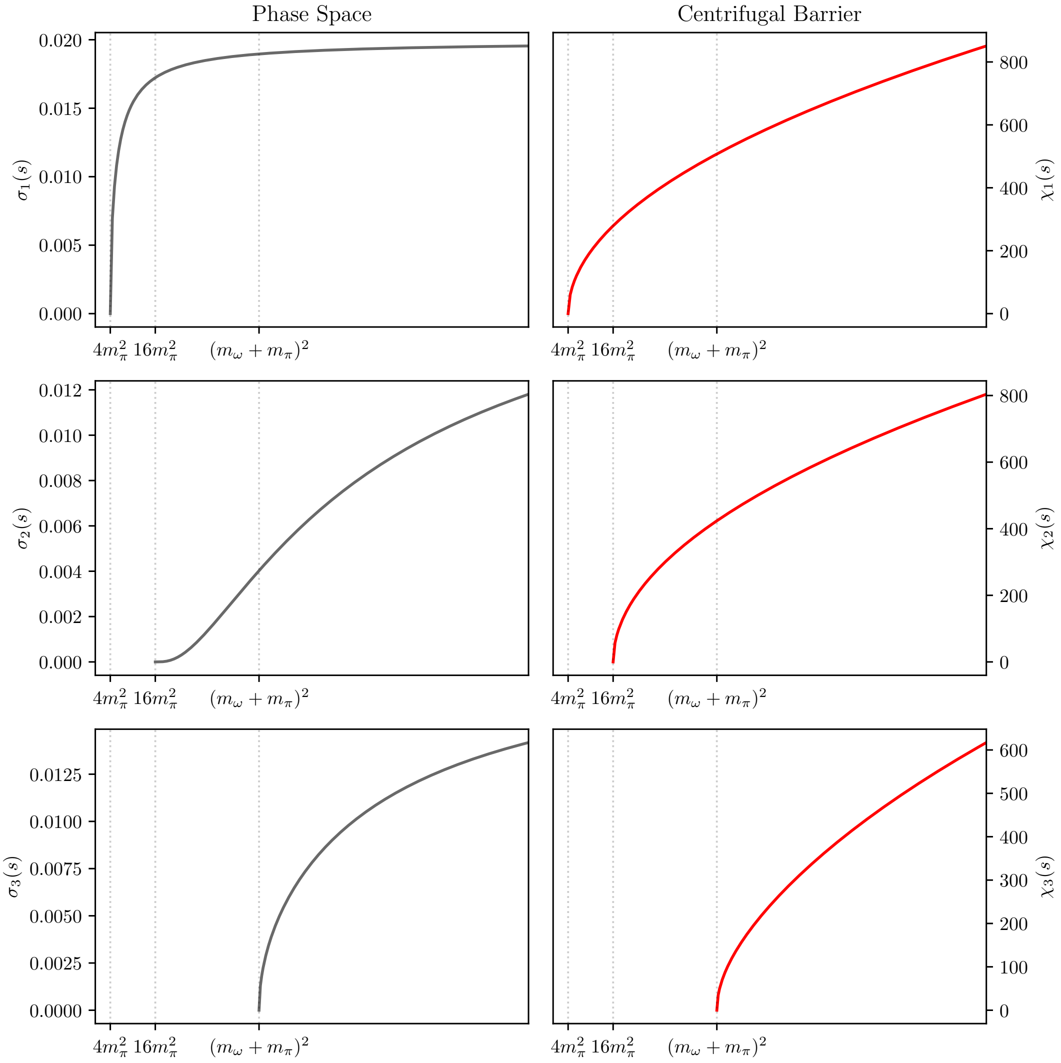

Figure 7: Phase space and centrifugal barrier factors for $2\pi, 4\pi$ and $\pi^0\omega$ channels.

The same vertex factor will be used for the $\pi^0\omega$ channel, which is again a 2-body channel with

$$
\begin{aligned}
E_{\text{thr},3} &= m_\pi + m_\omega \approx 922 \text{ MeV}, \\
\sigma_3(s) &= \frac{1}{16\pi}\sqrt{\left(1 - \frac{(m_\omega + m_\pi)^2}{s}\right)\left(1 - \frac{(m_\omega - m_\pi)^2}{s}\right)}, \\
\xi_3(s) &= \frac{1}{\sqrt{3}}\sqrt{\left(s - (m_\pi + m_\omega)^2\right)\left(s - (m_\pi - m_\omega)^2\right)/s}, \\
\Gamma_3(s) &= \frac{\Lambda^2}{\Lambda^2 + s},
\end{aligned} \tag{3.6}
$$

where we simply follow (3.1). Strictly speaking, the ω is not stable. However, its most dominant decay ($\omega \to 3\pi$ with a branching ratio of around 90% [PDG 2020]) is already taken into account, as the $\pi^0\omega$ channel is connected to the 4π channel within the model.

The phase space and the centrifugal barrier factors are plotted in Figure 7. One can notice the slow onset for the second channel due to the fact that the final state is 4-body.

With this, self-energies can be calculated. Figure 8 shows the plots for different values of Λ. There

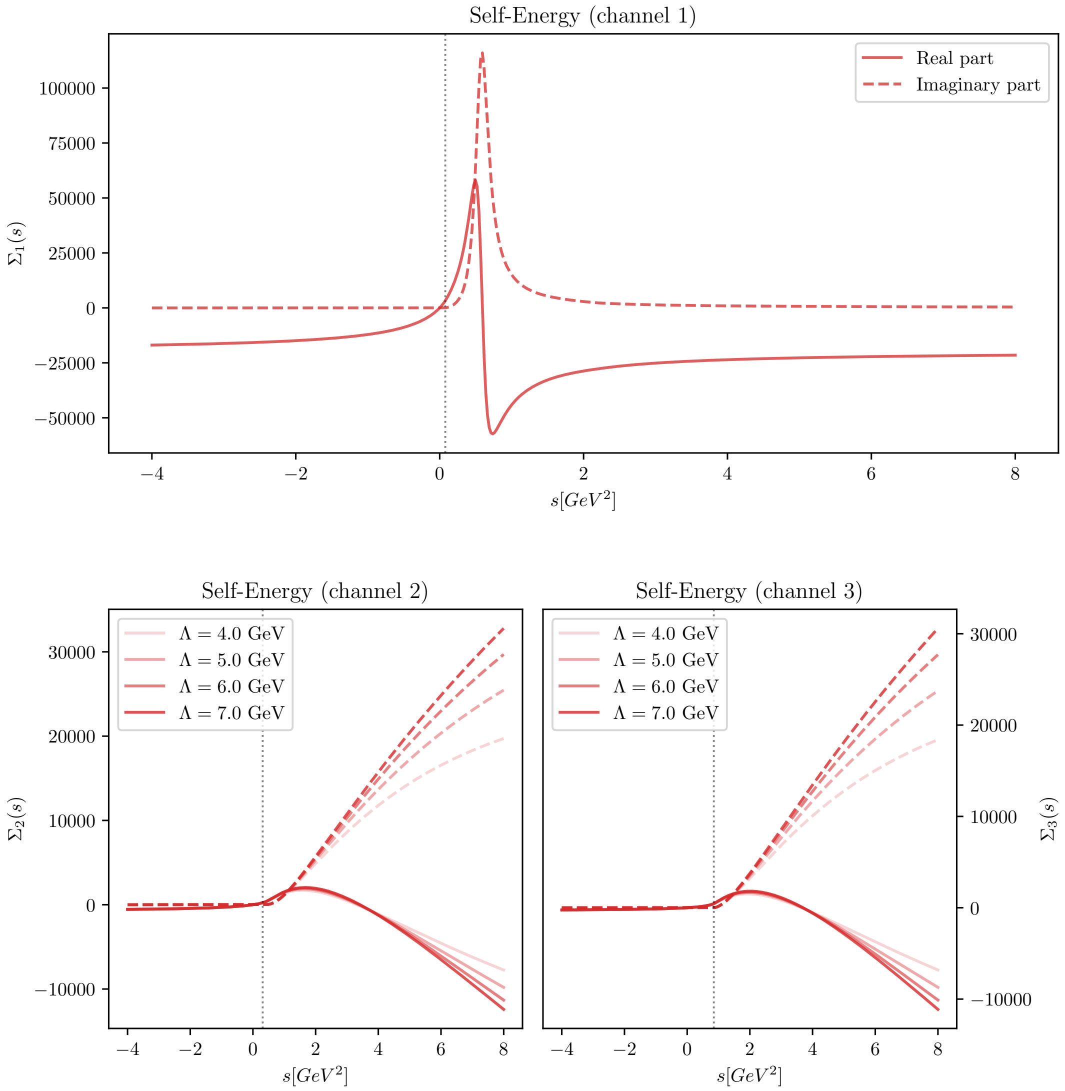

Figure 8: Self-energies calculated according to (2.47).

is a noticeable change in the curvature of the lines, but the overall shape does not change with the variation of Λ. On the plot of the first channel the contribution of the $\rho(770)$ to the self-energy is visible.

3.2 Data

3.2.1 The $\pi\pi$ P-wave phase shift

The $\pi\pi$ scattering amplitude can be parametrized using the so-called Roy equations [Roy 1971]. The maximum energy of validity of the Roy equations is 1.15 GeV. Above this region one could use purely phenomenological approaches (see e.g. [García-Martín et al. 2011]). Within the region of validity the parametrization can be supplemented by the so-called Regge analysis to provide a more precise input at high energies [Caprini et al. 2012]. The phase shifts of the Roy equation analysis of the Bern group adjusted to account for the vector form factor fits [Colangelo et al. 2019] is plotted in Figure 5 and used throughout this work.

3.2.2 The pion vector form factor

The pion vector form factor $F_V(s)$ can be extracted from the process $e^+e^- \to \pi^+\pi^-$ (see (3.2)) [KLOE 2005; SND 2005; CMD-2 2005, 2007; BaBaR 2012] or from the $\tau \to \pi^-\pi^0\nu_\tau$ decay [BELLE 2008]. We use the data set by the *BABAR* collaboration [BaBaR 2012] since it covers the largest energy range. The cross section was measured using the initial-state radiation technique. The data points are plotted in Figure 6.

3.2.3 The $e^+e^- \to \pi^0\omega$ cross section

The process $e^+e^- \to \pi^0\omega$ gives one of the most important contributions to the total hadronic cross section in the energy range of 1-2 GeV. However, ω being unstable, what is measured in the experiment are its decay products. Two of its most prominent decay modes are $\pi^+\pi^-\pi^0$ and $\pi^0\gamma$ with branching ratios [PDG 2020]

$$\begin{aligned}\Gamma_{\omega\to\pi^+\pi^-\pi^0}/\Gamma_\omega &= 89.2 \pm 0.7\%,\\ \Gamma_{\omega\to\pi^0\gamma}/\Gamma_\omega &= 8.40 \pm 0.22\%.\end{aligned} \tag{3.7}$$

The cross section of the process $e^+e^- \to \pi^0\omega \to \pi^+\pi^-2\pi^0$ was measured by the *BABAR* collaboration [BaBaR 2017] using the initial-state radiation technique, from the process $e^+e^- \to \pi^+\pi^-2\pi^0\gamma$.

Experiments conducted in Novosibirsk with the *CMD-2* [CMD-2 2003] and *SND* [SND 2000, 2016] detectors measure the cross section for $e^+e^- \to \pi^0\omega \to \pi^0\pi^0\gamma$. Even though the branching ratio of $\pi^0\gamma$ is about ten times smaller than that of 3π (3.7), the final state is easier to single out, in contrast to the 4π state, where one has to deal with a systematic uncertainty accompanied with non-trivial background subtraction.

The cross section $\sigma_{e^+e^-\to\pi^0\omega}$ can be obtained by taking the data from these experiments and dividing them by the relevant branching ratios from (3.7). The connection between the cross section and the pertinent form factor is given by (3.2). The data points are plotted in Figure 9.

Even though it is not used for fitting, the data for $\omega \to \pi^0 l^+l^-$ [NA60 2009, 2016; MAMI 2017] is worth mentioning here. For the discussion of the experimental evidence for the $\rho(770)$ in the $\pi^0\omega$ form factor data see e.g. [Schneider et al. 2012].

3.2.4 The elasticity η_1

At high energies elastic unitarity does not hold anymore. The parametrization of the partial wave scattering amplitude t_l is then given in terms of not one, but two real functions: the phase shift $\delta_l(s)$ and elasticity[1] $\eta_l(s)$. We already have $\delta_1(s)$ from [Caprini et al. 2012]. We will use the parametrization for $\eta_1(s)$ from [García-Martín et al. 2011], plotted in Figure 10. The parametrization is valid in the range $2m_K < E <$1420 MeV, where m_K is the mass of the kaon.

3.2.5 Cross section ratio r

Another interesting quantity is the following ratio

$$r = \frac{\sigma^{I=1}_{e^+e^-\to\text{non}-2\pi}}{\sigma_{e^+e^-\to\pi^+\pi^-}} \tag{3.8}$$

[1] Note, that some authors call this *in*elasticity. We will, however, use the term *elasticity*, since it is equal to 1 for elastic scattering.

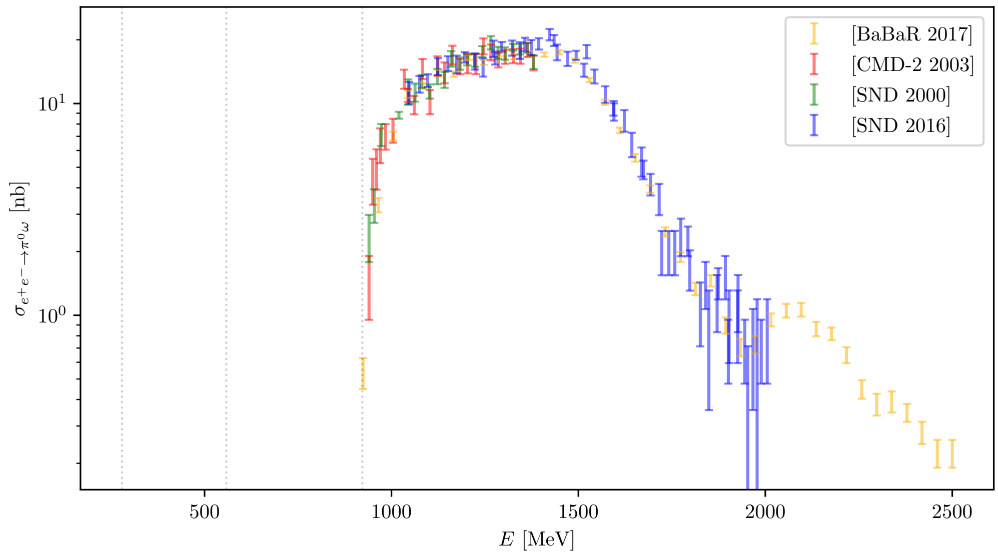

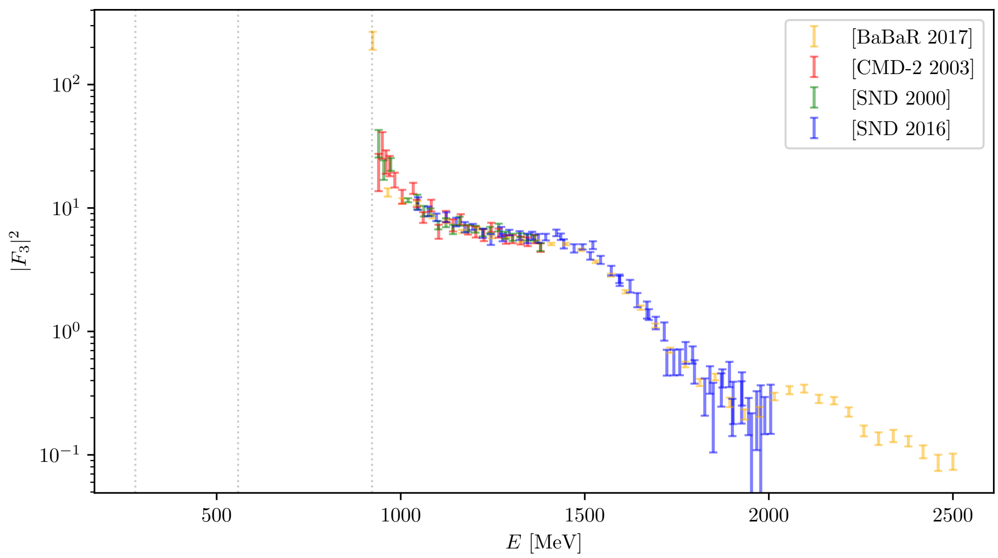

Figure 9: Cross sections for the process $e^+e^- \to \pi^0\omega$ and $|F_3|^2$, defined as in (3.2). The data is from [BaBaR 2017; CMD-2 2003; SND 2000, 2016].

between the total cross sections of e^+e^- to $I = 1$ non-2π channels over those to 2π. The data for energies in the range 820 MeV $< E <$ 1400 MeV is given in [Eidelman and Łukaszuk 2004] and is plotted in Figure 10.

We do not fit our model to any exclusive cross section data from the 4π channel. However, a combination of $\sigma_{e^+e^-\to\pi^+\pi^-}, \sigma_{e^+e^-\to\pi^0\omega}$ and r constrains the model so that the contribution from all channels is included. In this sense, we *are* fitting the model to the data from all three open channels.

3.3 Results

The fitting procedure was performed using MINUIT. MINUIT is a function minimization and error analysis software, originally written in Fortran [James and Roos 1975]. A modern version of MINUIT (now called MINUIT2) is ported to and maintained by ROOT [Hatlo et al. 2005]. The software has

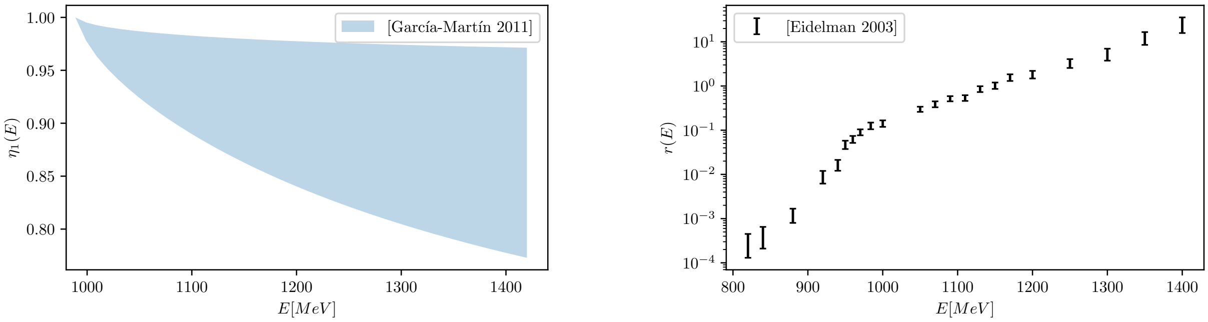

Figure 10: Elasticity η_1 (left) and cross-section ratio r (right).

$m_1 = 1313 \pm 13$ MeV	$m_2 = 2027 \pm 27$ MeV	$m_3 = 2860 \pm 51$ MeV
$g_{11} = -0.07 \pm 0.03$	$g_{12} = -5.33 \pm 0.19$	$g_{13} = 1.67 \pm 0.13$
$g_{21} = 0.12 \pm 0.48$	$g_{22} = 2.89 \pm 0.16$	$g_{23} = 25.0 \pm 1.5$
$g_{31} = -4.85 \pm 0.63$	$g_{32} = -24.0 \pm 0.07$	$g_{33} = -8.75 \pm 1.2$
$\alpha_1 = -0.56 \pm 0.01$	$\alpha_2 = -0.002 \pm 0.007$	$\alpha_3 = -0.14 \pm 0.03$
$c_2 = 12.9 \pm 1.0$	$c_3 = 3.13 \pm 0.25$	
$\kappa_\omega = -0.002 \pm 0.0008$	$\kappa_\phi = 0.0005 \pm 0.0024$	

Table 2: Results of the fit #1: χ^2/d.o.f. = 3.13 (*excluding* the r data set).

also been ported to Java and Python. We are using the Python version, called `iminuit` [Dembinski et al. 2020].

3.3.1 Fit #1: 3 channels, 3 resonances: issue with the ρ peak

The results of the fit for 3 channels $(2\pi, 4\pi, \pi^0\omega)$ and 3 resonances are given in Table 2. We will call this fit #1. The form factors for channels 1 and 3 are plotted on Figure 11. The systematic uncertainties attributed to the value of Λ in the vertices are represented by the width of the lines, which correspond to Λ in the range from 4 to 7 GeV. As expected from Figure 8, the model is sensitive to the value of Λ at high energies.

There are two things that we were unable to reproduce well during this procedure. First of all, there is no signal of the $\rho(770)$ in the $\pi^0\omega$ form factor. This is clearly visible in the plot. In the two-potential model described above, the contribution of the $\rho(770)$ resides in the Omnès function, which is used as a vertex of the first channel [Hanhart 2012]. Hence, in order for the third channel to couple with the $\rho(770)$ strongly enough (so that the peak is reproduced), the coupling with the first channel should be strong. We were unable to provide such a coupling with the resonance potential. Introducing contact terms between the channels in the potential could resolve this problem. While we do not have final results including the contact terms, the working fits look promising.

Secondly, the procedure was performed by excluding the data of the cross section ratio r. If one includes it in the calculation of χ^2, the value of the latter becomes orders of magnitudes bigger with the same model parameters (as given in Table 2). We were unable to reproduce sensible results with all data sets included in the minimization procedure.

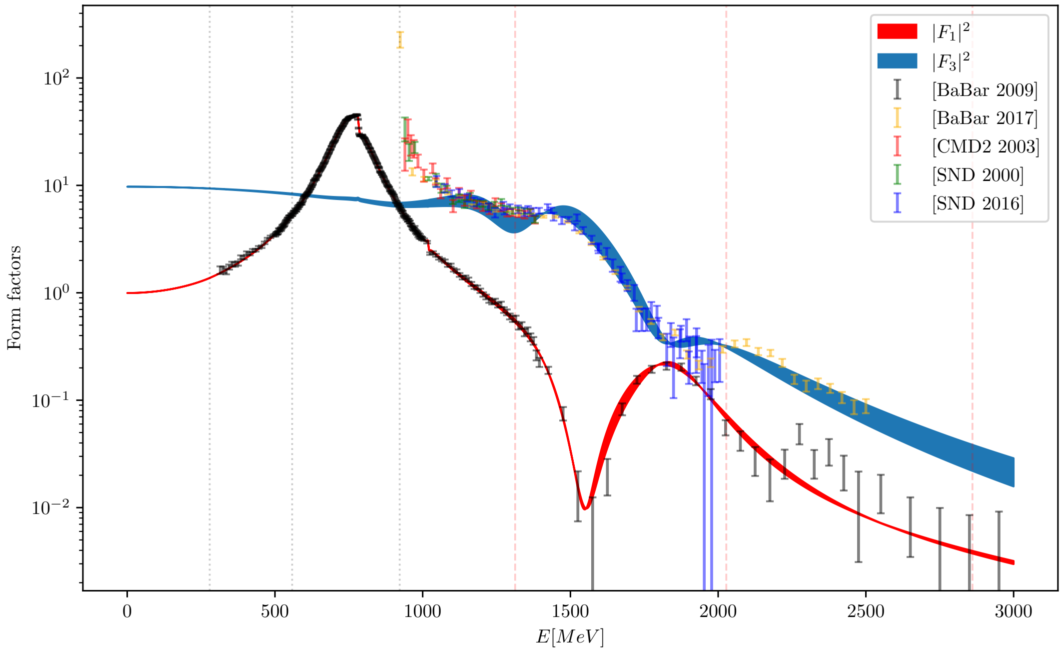

Figure 11: Fit #1: results for 3 channels and 3 resonances. Form factors for the 2π (red) and the $\pi^0\omega$ channel compared with the data. Dotted gray vertical lines are threshold energies and dashed red vertical lines are the masses of resonances. The width of the lines is due to the value of Λ, which we vary in the range from 4 GeV to 7 GeV.

$m_1 = 806 \pm 2$ MeV	$m_2 = 1667 \pm 23$ MeV	$m_3 = 2423 \pm 36$ MeV
$g_{11} = -6.0 \pm 0.3$	$g_{12} = -0.53 \pm 0.17$	$g_{13} = 1.59 \pm 0.22$
$g_{21} = -0.50 \pm 0.07$	$g_{22} = -4.11 \pm 0.07$	$g_{23} = -7.73 \pm 0.27$
$g_{31} = 4.29 \pm 0.32$	$g_{32} = -24.5 \pm 1.1$	$g_{33} = -24.8 \pm 1.4$
$\alpha_1 = -0.47 \pm 0.02$	$\alpha_2 = -0.343 \pm 0.004$	$\alpha_3 = 0.13 \pm 0.01$
$c_2 = -1.2 \pm 2$	$c_3 = 1.22 \pm 0.16$	
$\kappa_\omega = 0.020 \pm 0.009$	$\kappa_\phi = 0.001 \pm 0.004$	

Table 3: Results of the fit #2: χ^2/d.o.f. = 5.05 *excluding* the $\tilde{\delta}_1$ data set and 88.32 *including* it.

3.3.2 Fit #2: 3 channels, 3 resonances: without the input phase

One way to address the problem at hand is to move the contribution of the $\rho(770)$ from the input vertex to the model parameters. In other words, we can use the vertex function:

$$\Gamma_1(s) = \frac{\Lambda^2}{\Lambda^2 + s}. \tag{3.9}$$

This way all channels are treated on the same footing (all channels will directly couple to all resonances, $\rho(770)$ included). The scattering phase $\tilde{\delta}_1$ will still contribute, as it is part of the χ^2 in the minimization procedure. Thus we now study a unitarized multi-channel version of the Gounaris-Sakurai model [Gounaris and Sakurai 1968].

The results of the fit #2 are given in Table 3 and plotted in Figures 12 to 15.

Figure 12 shows the form factors. One can notice the $\rho(770)$ peak in both channels now. This peak is attributed to the first resonance of our model with bare mass $m_1 = 806 \pm 2$ MeV.

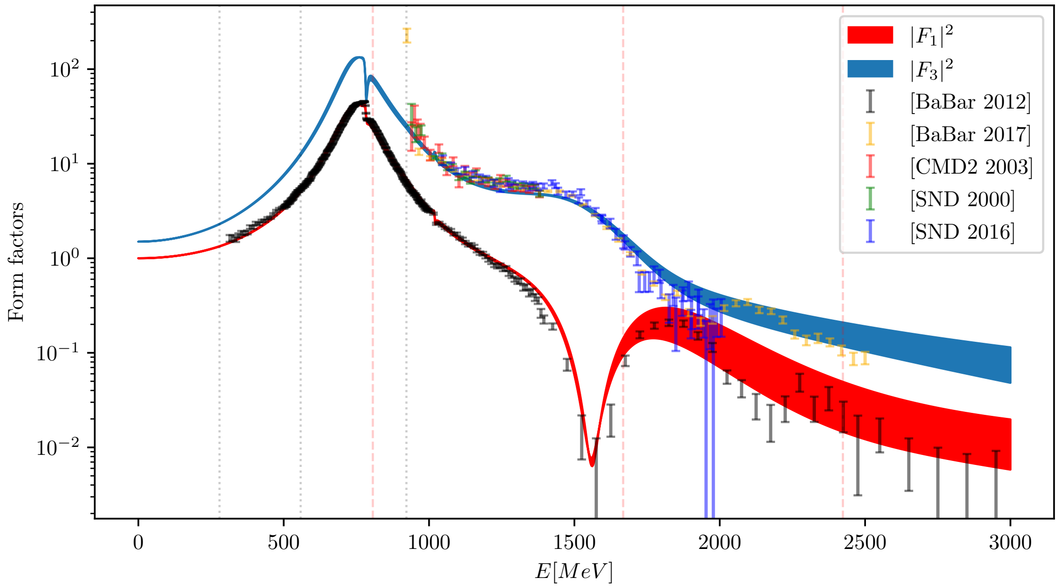

Figure 12: Fit #2: results for 3 channels and 3 resonances. Form factors for the 2π (red) and the $\pi^0\omega$ channel compared with the data. Dotted gray vertical lines are threshold energies and dashed red vertical lines are the masses of resonances. The width of the lines is due to the value of Λ, which we vary in the range from 4 GeV to 7 GeV.

The phases obtained with this method are plotted in Figure 13. The scattering and the form factor phases agree in the low energy region, as expected from the Watson's theorem. The scattering phase agrees to the parametrization from [Caprini et al. 2012] at low energies, but strongly deviates from it above the mass of the $\rho(770)$. The $\pi\pi$ scattering phases are known with excellent precision, such that the simple resonance model employed here is not enough to accurately reconstruct the line shape of the $\rho(770)$. This all leads to a significant increase of the χ^2.

Figure 14 shows the elasticity parameter compared with the parametrization from [García-Martín et al. 2011]. Physically, η must be bound between 0 and 1. The reason behind the little bump at the mass of ω is (2.54). As mentioned in the text, adding $\rho - \omega$ mixing in such a simplified way destroys unitarity. This is exactly what we observe, as the elasticity becomes greater than 1 at this point. There is another such bump (although, smaller and barely visible) at the mass of ϕ. However, these effects are tiny and well localized.

The non-$2\pi/2\pi$ cross section ratio r is plotted on Figure 15. The matching is quite good above the $\pi^0\omega$ threshold, but not so much below, where the only contributor should be the 4π channel. The fit could be improved if the 4π exclusive data is added to the χ^2. In addition, one could also employ more sophisticated phase space and/or centrifugal barrier factors for the 4π channel. In particular, the contribution of $a_1\pi$ intermediate state can be considered (see e.g. [Achasov and Kozhevnikov 2013]).

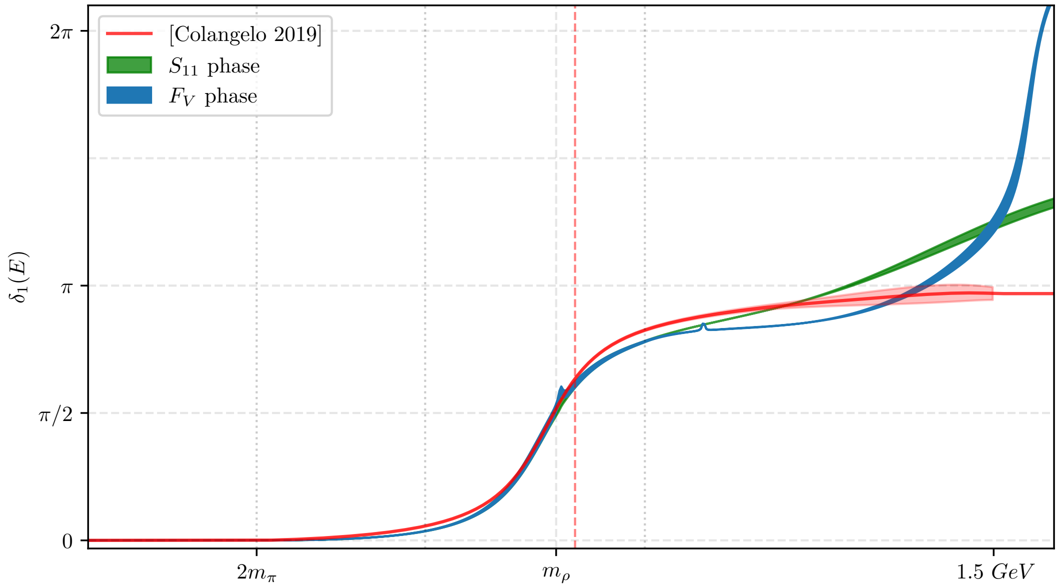

Figure 13: Fit #2: The scattering (green) and the form factor (blue) phases compared to $\tilde{\delta}_1$ from [Colangelo et al. 2019] (red). Dotted gray vertical lines are threshold energies and dashed red vertical lines are the masses of resonances. The width of the lines is due to the value of Λ, which we vary in the range from 4 GeV to 7 GeV.

4 Summary

In this work a two-potential formalism was presented, which parametrizes form factors in such a way that the principles of analyticity and unitarity are preserved [Hanhart 2012]. Additionally to the analysis of the original paper, here the exclusive $\pi^0\omega$ data was fitted. The formalism was applied to the pion vector form factor. The $\pi\pi$ scattering phases were used as input for low energies. A good description is found for the pion vector form factor in the neutral channel (including isospin-breaking effects, such as $\rho - \omega$ and $\rho - \phi$ mixing, as well as the mixing of ρ with the photon). However, we were unable to accurately describe the $e^+e^- \to \pi^0\omega$ cross section at low energies. In particular, the formalism does not provide a sufficiently strong coupling between the ρ and the $\pi^0\omega$ channel. The problem could be resolved by introducing contact terms to the potential. This, however, is a topic of further research and is not included within the scope of this work. Apart from that, no sensible results were obtained by including the e^+e^- to non-2π to 2π cross section ratio r in the fitting procedure.

Another fit was performed without using the input phases, but still including them in the cost function. The results show a significantly improved description of the $\pi^0\omega$ cross section as well as the cross section ratio r at the cost of the accuracy in the $\pi\pi$ scattering phase. The reason for this is the following: excluding the input phases, we now model both low- and high-energy regions using a resonance potential and therefore, employing a unitarized Gounaris-Sakurai model. This model is too simple (compared to the methods used e.g. in [Colangelo et al. 2001]) to accurately describe $\pi\pi$ scattering.

Within this work the $\pi^0\omega$ form factor was investigated in the production region, i.e. the data from $e^+e^- \to \pi^0\omega$ was considered. The decay region for the reaction $\omega \to \pi^0\gamma$ was not included in the fit. These two regions are usually modeled independently. Including the decay region into the fit could help simultaneously model the transition form factor at both low and high energies, which is a subject of active research.

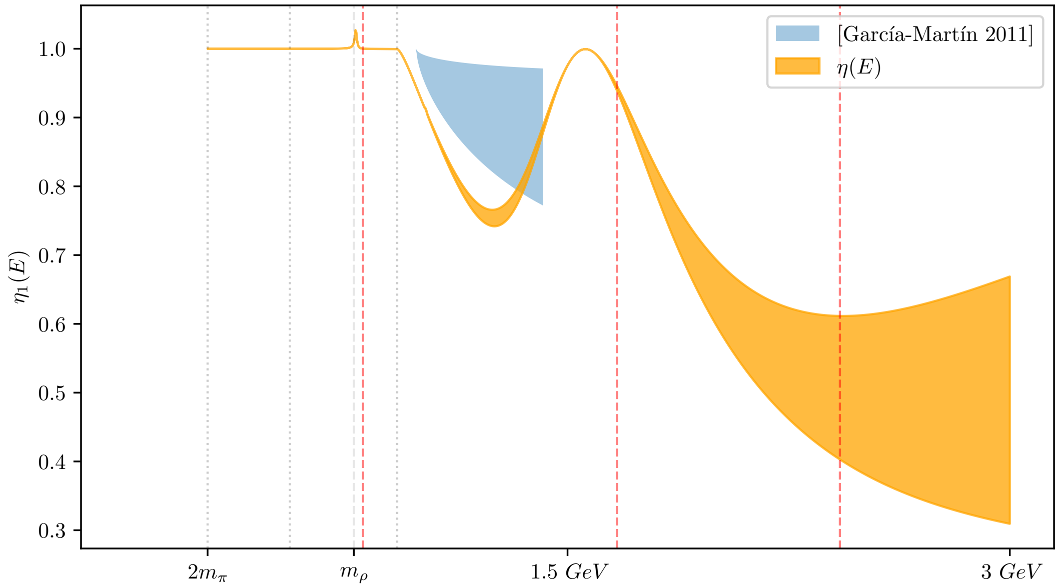

Figure 14: Fit #2: Elasticity parameter η_1 (yellow) compared to the parametrization given in [García-Martín et al. 2011] (light blue). Dotted gray vertical lines are threshold energies and dashed red vertical lines are the masses of resonances. The width of the lines is due to the value of Λ, which we vary in the range from 4 GeV to 7 GeV.

The cross-section ratio r predicted by our model deviates from the experimental values between the 4π and $\pi^0\omega$ thresholds. This discrepancy could be improved by adding exclusive 4π data into the fitting procedure. The analysis could be improved with the ongoing research of the amplitude of the reaction $e^+e^- \to 4\pi$. In particular, the $a_1\pi$ intermediate state could be included into the model (for the role of $a_1(1260)$ in the 4π processes see e.g. [CMD-2 1999; Bondar et al. 1999]). We leave these improvement strategies to the future studies.

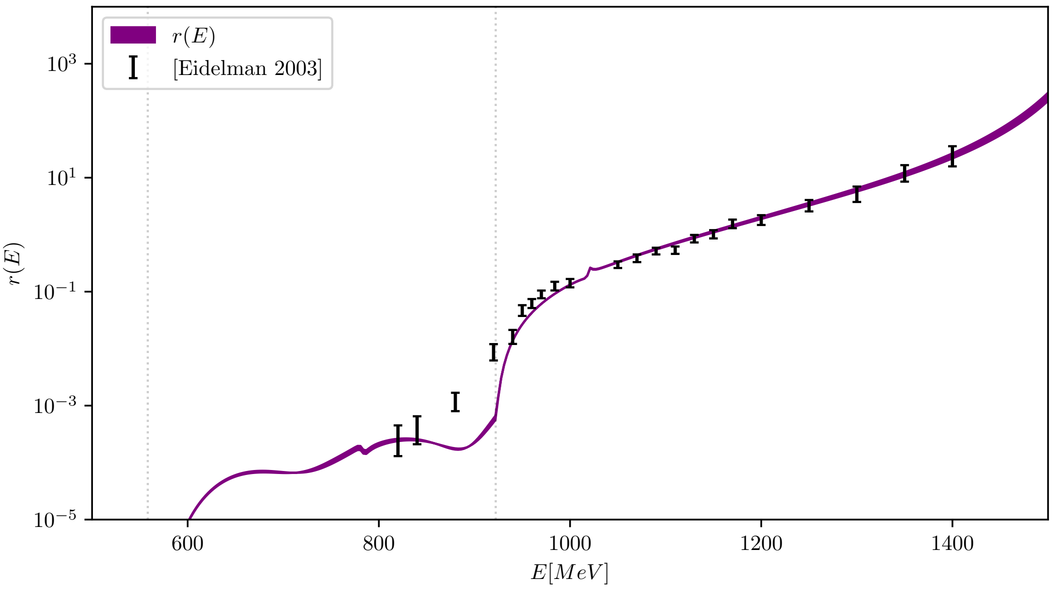

Figure 15: Fit #2: The non-2π to 2π cross section ratio compared with the data from [Eidelman and Łukaszuk 2004]. Dotted gray vertical lines are threshold energies. The width of the lines is due to the value of Λ, which we vary in the range from 4 GeV to 7 GeV.

A Discontinuities

A.1 Discontinuity of the elastic transition matrix

The elastic transition matrix $\tilde{T}$ describes the elastic scattering of a two-pion system (see Figure 4). Below the first inelastic threshold its discontinuity comes from the same two-pion intermediate state:

disc 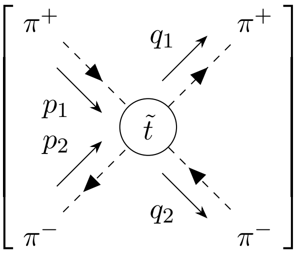

$$= i\int (2\pi)^4 d\Phi_2\Big|_{k_1,k_2}$$

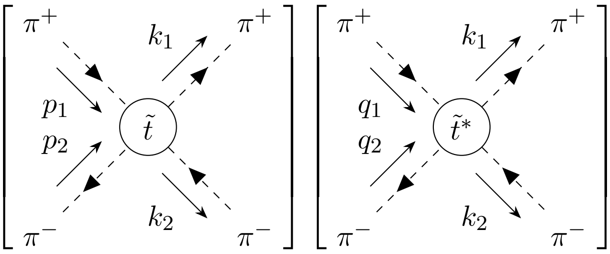

$$= i\int \frac{\delta^{(4)}(q_1+q_2-k_1-k_2)}{(2\pi)^2}\frac{d^3k_1}{2E_{\vec{k}_1}}\frac{d^3k_2}{2E_{\vec{k}_2}}$$

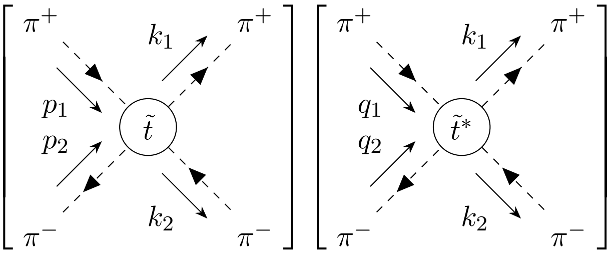

$$\begin{aligned}
&= i\int \frac{\delta^{(4)}(q_1+q_2-k_1-k_2)}{(2\pi)^2}\frac{d^3k_1}{2E_{\vec{k}_1}}\frac{d^3k_2}{2E_{\vec{k}_2}}\left[\tilde{t}(s,\cos\theta_p)\right]\left[\tilde{t}^*(s,\cos\theta_q)\right]\Bigg|^{\theta_p=\angle(\vec{k}_1,\vec{p}_1)}_{\theta_q=\angle(\vec{k}_1,\vec{q}_1)} \\
&= i\int \frac{\delta(\sqrt{s}-2E_{\vec{k}_1})}{(2\pi)^2}\frac{d^3k_1}{(2E_{\vec{k}_1})^2}\left[\tilde{t}(s,\cos\theta_p)\right]\left[\tilde{t}^*(s,\cos\theta_q)\right] \\
&= i\int \frac{\delta(\sqrt{s}-2E_{\vec{k}_1})}{(2\pi)^2}\frac{d\Omega_s\,|\vec{k}_1|^2 d|\vec{k}_1|}{(2E_{\vec{k}_1})^2}\left[\tilde{t}(s,\cos\theta_p)\right]\left[\tilde{t}^*(s,\cos\theta_q)\right] \\
&= i\int \frac{\delta\left(\sqrt{s}-2\sqrt{m_\pi^2+|\vec{k}_1|^2}\right)}{(2\pi)^2}\frac{d\Omega_s\,|\vec{k}_1|^2 d|\vec{k}_1|}{(2\sqrt{m_\pi^2+|\vec{k}_1|^2})^2}\left[\tilde{t}(s,\cos\theta_p)\right]\left[\tilde{t}^*(s,\cos\theta_q)\right] \\
&= i\frac{\sqrt{s}}{(2\pi)^2 4|\vec{k}_1|}\frac{|\vec{k}_1|^2}{(\sqrt{s})^2}\int d\Omega_s\left[\tilde{t}(s,\cos\theta_p)\right]\left[\tilde{t}^*(s,\cos\theta_q)\right]\Bigg|_{|\vec{k}_1|=\sqrt{s-4m_\pi^2}/2} \\
&= \frac{i}{16\pi}\sqrt{1-\frac{4m_\pi^2}{s}}\int_{-1}^{1} d\cos\theta_q\left[\tilde{t}(s,\cos\theta_p)\right]\left[\tilde{t}^*(s,\cos\theta_q)\right].
\end{aligned} \tag{A.1}$$

We define $\theta_{pq} = \theta_p - \theta_q = \angle(\vec{p}_1, \vec{q}_1)$. Thus, we are dealing with the integral:

$$\int_{-1}^{1} d\cos\theta_q\left[\tilde{t}(s,\cos(\theta_{pq}+\theta_q))\right]\left[\tilde{t}^*(s,\cos\theta_q)\right]. \tag{A.2}$$

The transition amplitude can be expanded using the partial-wave decomposition:

$$\begin{aligned}
\tilde{t}(s,\cos\theta) &= \sum_l (2l+1)P_l(\cos\theta)t_l(s) \\
&= P_0(\cos\theta)\tilde{t}_0(s) + 3P_1(\cos\theta)\tilde{t}_1(s) + 5P_2(\cos\theta)\tilde{t}_2(s) + \ldots
\end{aligned}$$

$$\begin{aligned}&\text{[For P-wave only } l=1 \text{ term survives.]}\\ &\tilde{t}(s,\cos\theta) = 3P_1(\cos\theta)\tilde{t}_1(s) = 3\cos\theta\ \tilde{t}_1(s).\end{aligned} \tag{A.3}$$

So, for the P-wave one needs to take

$$\begin{aligned}
&\int_{-1}^{1} d\cos\theta_q \left[\cos(\theta_{pq}+\theta_q)\tilde{t}_1(s)\right]\left[\cos\theta_q \tilde{t}_1^*(s)\right] = \\
&\quad = 9\int_{-1}^{1} d\cos\theta_q \left[\cos(\theta_{pq})\cos(\theta_q) - \sin(\theta_{pq})\sin(\theta_q))\tilde{t}_1(s)\right]\left[\cos\theta_q \tilde{t}_1^*(s)\right]\\
&\quad = 9|\tilde{t}_1(s)|^2 \int_{-1}^{1} d\cos\theta_q \left[\cos(\theta_{pq})\cos(\theta_q) - \sin(\theta_{pq})\sin(\theta_q))\right]\left[\cos\theta_q\right]\\
&\quad = 9|\tilde{t}_1(s)|^2 \left(\cos(\theta_{pq})\int_{-1}^{1}\cos^2(\theta_q)d\cos(\theta_q) - \sin(\theta_{pq})\int_{-1}^{1}\sin(\theta_q)\cos(\theta_q)d\cos\theta_q\right)\\
&\quad = 9|\tilde{t}_1(s)|^2 \left(\cos(\theta_{pq})\int_{-1}^{1} z^2 dz - \sin(\theta_{pq})\int_{-1}^{1} z\sqrt{1-z^2}dz\right)\\
&\quad = 9|\tilde{t}_1(s)|^2 \left(\cos(\theta_{pq})\frac{2}{3} - \sin(\theta_{pq})\cdot 0\right)\\
&\quad = 6|\tilde{t}_1(s)|^2\cos(\theta_{pq}).
\end{aligned} \tag{A.4}$$

Finally,

$$\begin{aligned}
\text{disc}\left[3\cos(\theta_{pq})\tilde{t}_1(s)\right] &= \frac{i}{16\pi}\sqrt{1-\frac{4m_\pi^2}{s}}\cdot 6|\tilde{t}_1(s)|^2\cos(\theta_{pq})\\
\implies \text{disc}\left[\tilde{t}_1(s)\right] &= \frac{i}{8\pi}\sqrt{1-\frac{4m_\pi^2}{s}}\cdot|\tilde{t}_1(s)|^2 = 2i\sigma(s)|\tilde{t}_1(s)|^2,
\end{aligned} \tag{A.5}$$

where

$$\sigma(s) = \frac{1}{16\pi}\sqrt{1-\frac{4m_\pi^2}{s}}, \tag{A.6}$$

which leads to

$$\tilde{t}_1(s) = \frac{1}{\sigma(s)}\sin(\tilde{\delta}_1(s))e^{i\tilde{\delta}_1(s)}. \tag{A.7}$$

A.2 Discontinuity of the form factor due to the elastic cut

The first contribution to the discontinuity of the pion vector form factor is the existence of the 2π intermediate state. The discontinuity can be expressed according to the Cutkosky cutting rule (see Figure 4):

$$\mathrm{disc}$$

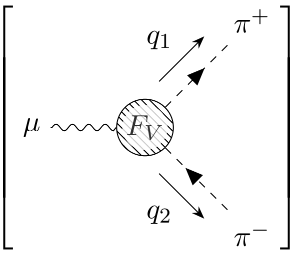

$$= i\int (2\pi)^4 d\Phi_2\Big|_{k_1,k_2}$$

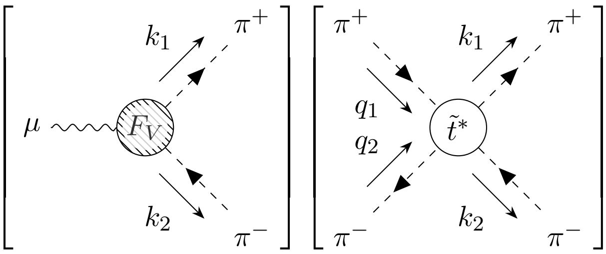

$$= i\int \frac{\delta^{(4)}(q_1+q_2-k_1-k_2)}{(2\pi)^2}\frac{d^3k_1}{2E_{\vec{k}_1}}\frac{d^3k_2}{2E_{\vec{k}_2}}$$

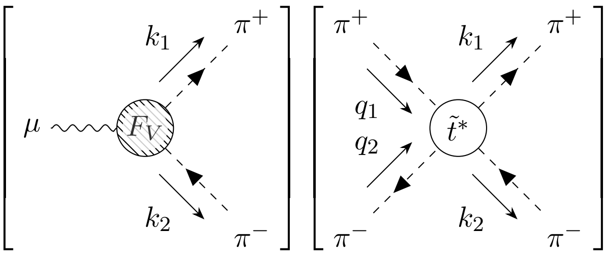

$$\begin{aligned}
&= i\int \frac{\delta^{(4)}(q_1+q_2-k_1-k_2)}{(2\pi)^2}\frac{d^3k_1}{2E_{\vec{k}_1}}\frac{d^3k_2}{2E_{\vec{k}_2}}\Big[(k_1-k_2)^\mu F_V(s)\Big]\Big[\tilde{t}^*(s,\cos\theta_q)\Big]\Big|_{\theta_q=\angle(\vec{k}_1,\vec{q}_1)}\\
&= i\int \frac{\delta(\sqrt{s}-2E_{\vec{k}_1})}{(2\pi)^2}\frac{d^3k_1}{(2E_{\vec{k}_1})^2}\Big[(2k_1-q_1-q_2)^\mu F_V(s)\Big]\Big[\tilde{t}^*(s,\cos\theta_q)\Big]\\
&= i\int \frac{\delta(\sqrt{s}-2E_{\vec{k}_1})}{(2\pi)^2}\frac{d\Omega_s\;|\vec{k}_1|^2 d|\vec{k}_1|}{(2E_{\vec{k}_1})^2}\Big[(2k_1-q_1-q_2)^\mu F_V(s)\Big]\Big[\tilde{t}^*(s,\cos\theta_q)\Big]\\
&= i\int \frac{\delta\left(\sqrt{s}-2\sqrt{m_\pi^2+|\vec{k}_1|^2}\right)}{(2\pi)^2}\frac{d\Omega_s\;|\vec{k}_1|^2 d|\vec{k}_1|}{(2\sqrt{m_\pi^2+|\vec{k}_1|^2})^2}\Big[(2k_1-q_1-q_2)^\mu F_V(s)\Big]\Big[\tilde{t}^*(s,\cos\theta_q)\Big]\\
&= i\frac{\sqrt{s}}{(2\pi)^2 4|\vec{k}_1|}\frac{|\vec{k}_1|^2}{(\sqrt{s})^2}F_V(s)\int d\Omega_s\Big[(2k_1-q_1-q_2)^\mu\Big]\Big[\tilde{t}^*(s,\cos\theta_q)\Big]\Bigg|_{|\vec{k}_1|=\sqrt{s-4m_\pi^2}/2}\\
&= \frac{i}{4(2\pi)^2}\frac{|\vec{k}_1|}{\sqrt{s}}F_V(s)\int d\Omega_s\Big[(2k_1-q_1-q_2)^\mu\Big]\Big[\tilde{t}^*(s,\cos\theta_q)\Big]\Bigg|_{|\vec{k}_1|=\sqrt{s-4m_\pi^2}/2}\\
&= \frac{i}{16\pi}\sqrt{1-\frac{4m_\pi^2}{s}}F_V(s)\int_{-1}^{1} d\cos\theta_q\Big[(2k_1-q_1-q_2)^\mu\Big]\Big[\tilde{t}^*(s,\cos\theta_q)\Big]\Bigg|_{|\vec{k}_1|=\sqrt{s-4m_\pi^2}/2}.
\end{aligned} \tag{A.8}$$

One needs to take the angular integral

$$I^\mu = \int_{-1}^{1} d\cos\theta_q\Big[(2k_1-q_1-q_2)^\mu\Big]\Big[\tilde{t}^*(s,\cos\theta_q)\Big]\Bigg|_{|\vec{k}_1|=\sqrt{s-4m_\pi^2}/2}. \tag{A.9}$$

The only relevant four-vectors we have here are q_1 and q_2. Therefore, we introduce the ansatz:

$$I^\mu = L_1(q_1+q_2)^\mu + L_2(q_1-q_2)^\mu. \tag{A.10}$$

Note, that

$$
\begin{aligned}
&(2k_1 - q_1 - q_2)^\mu (q_1 + q_2)_\mu = 2k_1 \cdot (q_1 + q_2) - (q_1 + q_2)^2 = s - s = 0, \\
&(2k_1 - q_1 - q_2)^\mu (q_1 - q_2)_\mu = 2k_1 \cdot (q_1 - q_2) - (q_1 + q_2) \cdot (q_1 - q_2) = (s - 4m_\pi^2) \cos\theta_q.
\end{aligned} \tag{A.11}
$$

If one now contracts I^μ with $(q_1 \pm q_2)_\mu$, we obtain

$$
\begin{aligned}
I^\mu (q_1 + q_2)_\mu &= L_1 s = 0 \implies L_1 = 0, \\
I^\mu (q_1 - q_2)_\mu &= L_2 (s - 4m_\pi^2) = \int_{-1}^{1} d\cos\theta_q \Big[(s - 4m_\pi^2)\cos\theta_q\Big] \Big[\tilde{t}^*(s, \cos\theta_q)\Big], \\
\implies L_2 &= \int_{-1}^{1} d\cos\theta_q \Big[\cos\theta_q\Big] \Big[\tilde{t}^*(s, \cos\theta_q)\Big].
\end{aligned} \tag{A.12}
$$

For the P-wave,

$$
\begin{aligned}
L_2 &= \tilde{t}_1^*(s) \int_{-1}^{1} 3\cos^2\theta_q \; d\cos\theta_q = 2\tilde{t}_1^*(s), \\
\implies I^\mu &= 2\tilde{t}_1^*(s)(q_1 - q_2)^\mu, \\
\implies \mathrm{disc}\,[F_V(s)] &= \frac{i}{8\pi}\sqrt{1 - \frac{4m_\pi^2}{s}}\,\tilde{t}_1^*(s) F_V(s) = 2i\sigma(s)\tilde{t}_1^*(s) F_V(s),
\end{aligned} \tag{A.13}
$$

where

$$
\sigma(s) = \frac{1}{16\pi}\sqrt{1 - \frac{4m_\pi^2}{s}}. \tag{A.14}
$$

B Invariant amplitudes

B.1 $e^+e^- \to \pi^+\pi^-$

Next we consider the process $e^+e^- \to \pi^+\pi^-$, described by the following diagram:

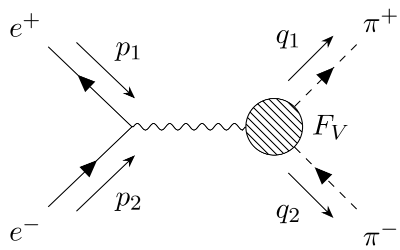

We define the Mandelstam variables as follows:

$$\begin{aligned} s &= (p_1+p_2)^2 = (q_1+q_2)^2, \\ t &= (p_1-q_1)^2 = (p_2-q_2)^2, \\ u &= (p_1-q_2)^2 = (p_2-q_1)^2. \end{aligned} \tag{B.1}$$

Apart from that, let us define

$$\begin{aligned} k &= p_1+p_2 = q_1+q_2, \\ l &= p_1-p_2, \quad l' = q_1-q_2. \end{aligned} \tag{B.2}$$

The invariant amplitude for this diagram is

$$\begin{aligned} i\mathcal{M} &= \bar{v}^s(p_1)(-ie\gamma^\mu)u^r(p_2)\frac{-ig_{\mu\nu}}{(p_1+p_2)^2}(ie)(q_1-q_2)^\nu F_V(s) \\ &= -i\frac{e^2}{s}\bar{v}^s(p_1)\gamma^\mu u^r(p_2)l'_\mu F_V(s). \end{aligned} \tag{B.3}$$

Taking the absolute value squared,

$$\begin{aligned} |\mathcal{M}|^2 &= \left(\frac{e^2}{s}\right)^2 \left(\bar{v}^s(p_1)\gamma^\mu u^r(p_2)\right)^* \left(\bar{v}^s(p_1)\gamma^\nu u^r(p_2)\right) l'_\mu l'_\nu |F_V(s)|^2 \\ &= \left(\frac{e^2}{s}\right)^2 \left(\bar{u}^r(p_2)\gamma^\mu v^s(p_1)\right)\left(\bar{v}^s(p_1)\gamma^\nu u^r(p_2)\right) l'_\mu l'_\nu |F_V(s)|^2. \end{aligned} \tag{B.4}$$

Averaging over all initial spin states,

$$\begin{aligned} \overline{|\mathcal{M}|^2} &= \frac{1}{4}\sum_{s,r}\left(\frac{e^2}{s}\right)^2 \left(\bar{u}^r(p_2)\gamma^\mu v^s(p_1)\right)\left(\bar{v}^s(p_1)\gamma^\nu u^r(p_2)\right) l'_\mu l'_\nu |F_V(s)|^2 \\ &= \frac{1}{4}\sum_{s,r}\left(\frac{e^2}{s}\right)^2 \left(\bar{u}^r_\alpha(p_2)\gamma^\mu_{\alpha\beta}v^s_\beta(p_1)\right)\left(\bar{v}^s_\rho(p_1)\gamma^\nu_{\rho\sigma}u^r_\sigma(p_2)\right) l'_\mu l'_\nu |F_V(s)|^2 \\ &= \frac{1}{4}\sum_{s,r}\left(\frac{e^2}{s}\right)^2 \left(v^s_\beta(p_1)\bar{v}^s_\rho(p_1)u^r_\sigma(p_2)\bar{u}^r_\alpha(p_2)\gamma^\mu_{\alpha\beta}\gamma^\nu_{\rho\sigma}\right) l'_\mu l'_\nu |F_V(s)|^2 \end{aligned}$$

$$= \frac{1}{4}\left(\frac{e^2}{s}\right)^2 \left(\left(\not{p}_1 - m_e\right)_{\beta\rho}\left(\not{p}_2 + m_e\right)_{\sigma\alpha}\gamma^{\mu}_{\alpha\beta}\gamma^{\nu}_{\rho\sigma}\right) l'_{\mu} l'_{\nu} |F_V(s)|^2$$
$$= \frac{1}{4}\left(\frac{e^2}{s}\right)^2 \mathrm{tr}\left(\gamma^{\mu}\left(\not{p}_1 - m_e\right)\gamma^{\nu}\left(\not{p}_2 + m_e\right)\right) l'_{\mu} l'_{\nu} |F_V(s)|^2. \tag{B.5}$$

We are going to need the result of this trace in other calculations, so let us compute separately:

$$\begin{aligned}
\frac{1}{4}\mathrm{tr}\left(\gamma^{\mu}\left(\not{p}_1 - m_e\right)\gamma^{\nu}\left(\not{p}_2 + m_e\right)\right) &= \left(p_1^{\mu}p_2^{\nu} + p_1^{\nu}p_2^{\mu} - \frac{k^2}{2}g^{\mu\nu}\right) \\
&= \left(\frac{(k+l)^{\mu}(k-l)^{\nu}}{4} + \frac{(k+l)^{\nu}(k-l)^{\mu}}{4} - \frac{k^2}{2}g^{\mu\nu}\right) \\
&= \left(\frac{k^{\mu}k^{\nu}}{2} - \frac{l^{\mu}l^{\nu}}{2} - \frac{k^2}{2}g^{\mu\nu}\right) \\
&= -\frac{1}{2}\Big(\left(k^2 g^{\mu\nu} - k^{\mu}k^{\nu}\right) + \left(l^{\mu}l^{\nu}\right)\Big).
\end{aligned} \tag{B.6}$$

This can be interpreted as the sum of two projection operators: $\left(k^2 g^{\mu\nu} - k^{\mu}k^{\nu}\right)$ projects in the direction transverse to k (which is the photon momentum) and $(l^{\mu}l^{\nu})$ projects in the direction longitudinal to l (which is, by construction, transverse to k). In other words, the leptonic current is transverse to the photon momentum. Plugging this back into (B.5),

$$\begin{aligned}
\overline{|\mathcal{M}|^2} &= -\frac{1}{2}\left(\frac{e^2}{s}\right)^2 \Big(\left(k^2 g^{\mu\nu} - k^{\mu}k^{\nu}\right) + \left(l^{\mu}l^{\nu}\right)\Big) l'_{\mu} l'_{\nu} |F_V(s)|^2 \\
&= -\frac{1}{2}\left(\frac{e^2}{s}\right)^2 \left(s\left(l'\right)^2 + \left(l\cdot l'\right)^2\right)|F_V(s)|^2 \\
&= -\frac{1}{2}\left(\frac{e^2}{s}\right)^2 \left(s\left(4m_\pi^2 - s\right) + (t-u)^2\right)|F_V(s)|^2 \\
&= +\frac{1}{2}\left(\frac{e^2}{s}\right)^2 \Big(\underbrace{s\left(s - 4m_\pi^2\right)}_{\lambda(s,m_\pi^2,m_\pi^2)} - \kappa^2(s)\cos^2(\theta_s)\Big)|F_V(s)|^2.
\end{aligned} \tag{B.7}$$

In the last equality we have used the definition of the scattering angle:

$$\cos(\theta_s) = \frac{t-u}{\kappa(s)},$$
$$\text{where} \quad \kappa(s) = \frac{\lambda^{1/2}(s,m_\pi^2,m_\pi^2)\lambda^{1/2}(s,m_e^2,m_e^2)}{s}. \tag{B.8}$$

So,

$$\begin{aligned}
\overline{|\mathcal{M}|^2} &= \frac{1}{2}\left(\frac{e^2}{s}\right)^2 \left(\lambda(s,m_\pi^2,m_\pi^2) - \lambda(s,m_\pi^2,m_\pi^2)\lambda(s,m_e^2,m_e^2)\frac{1}{s^2}\cos^2(\theta_s)\right)|F_V(s)|^2 \\
&= \frac{1}{2}\left(\frac{e^2}{s}\right)^2 \lambda(s,m_\pi^2,m_\pi^2)\left(1 - \frac{\lambda(s,m_e^2,m_e^2)}{s^2}\cos^2(\theta_s)\right)|F_V(s)|^2.
\end{aligned} \tag{B.9}$$

Integrating $\overline{|\mathcal{M}|^2}$ over the solid angle, one obtains:

$$\int \overline{|\mathcal{M}|^2} d\Omega = (2\pi)\int_{-1}^{+1}\left(\frac{e^2}{s}\right)^2 \lambda(s,m_\pi^2,m_\pi^2)\frac{1}{2}\left(1 - \frac{\lambda(s,m_e^2,m_e^2)}{s^2}\cos^2(\theta_s)\right)|F_V(s)|^2 d\cos(\theta_s)$$

$$= \frac{2\pi e^4}{s^2}\lambda(s,m_\pi^2,m_\pi^2)\underbrace{\left(1-\frac{1}{3}\frac{\lambda(s,m_e^2,m_e^2)}{s^2}\right)}_{=2/3 \text{ for } m_e \ll s}|F_V(s)|^2. \tag{B.10}$$

Defining

$$\begin{aligned}[\xi_1(s)]^2 &= \frac{1}{3}\frac{\lambda(s,m_\pi^2,m_\pi^2)}{s},\\ [\xi_{e^+e^-}(s)]^2 &= s+2m_e^2,\end{aligned} \tag{B.11}$$

we have

$$\int \overline{|\mathcal{M}|^2}d\Omega = (4\pi)e^2[\xi_{e^+e^-}(s)]^2\frac{1}{s^2}e^2[\xi_1(s)]^2|F_V(s)|^2. \tag{B.12}$$

Using (2.14), one obtains

$$\begin{aligned}\sigma_{e^+e^-\to\pi^+\pi^-} &= \frac{1}{64\pi^2}\frac{\lambda^{1/2}(s,m_\pi^2,m_\pi^2)}{\lambda^{1/2}(s,m_e^2,m_e^2)}\frac{1}{s}\int\overline{|\mathcal{M}|^2}d\Omega\\ &= \frac{2\pi e^4}{64\pi^2 s^3}\frac{\lambda^{3/2}(s,m_\pi^2,m_\pi^2)}{\lambda^{1/2}(s,m_e^2,m_e^2)}\left(1-\frac{1}{3}\frac{\lambda(s,m_e^2,m_e^2)}{s^2}\right)|F_V(s)|^2\\ \xrightarrow[\alpha=e^2/4\pi]{m_e^2\ll s} &= \frac{32\pi^3\alpha^2}{64\pi^2 s^3}\frac{\lambda^{3/2}(s,m_\pi^2,m_\pi^2)}{s}\left(1-\frac{1}{3}\right)|F_V(s)|^2\\ &= \frac{\pi\alpha^2}{3}\frac{\lambda^{3/2}(s,m_\pi^2,m_\pi^2)}{s^4}\underbrace{|F_V(s)|^2}_{|F_1(s)|^2}.\end{aligned} \tag{B.13}$$

B.2 $e^+e^- \to \pi^0\omega$

Next up, we have $e^-e^+ \to \pi^0\omega$.

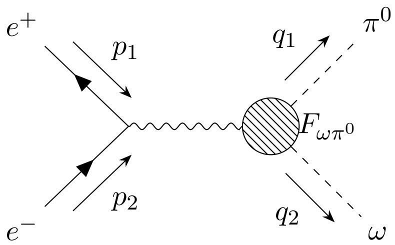

We define the Mandelstam variables similarly:

$$\begin{aligned}s &= (p_1+p_2)^2 = (q_1+q_2)^2,\\ t &= (p_1-q_1)^2 = (p_2-q_2)^2,\\ u &= (p_1-q_2)^2 = (p_2-q_1)^2,\end{aligned} \tag{B.14}$$

Also,

$$\begin{aligned}k &= p_1+p_2 = q_1+q_2,\\ l &= p_1-p_2, \quad l' = q_1-q_2.\end{aligned} \tag{B.15}$$

The invariant amplitude for this diagram can be written [Schneider 2012] as

$$\begin{aligned} i\mathcal{M}_3 &= \bar{v}^s(p_1)(-ie\gamma^\mu)u^r(p_2)\frac{-i}{(p_1+p_2)^2}(-ie)\epsilon_{\mu\nu\alpha\beta}n^\nu(q_2)q_1^\alpha(q_1+q_2)^\beta f_{\omega\pi^0}(s) \\ \xrightarrow[p_1+p_2=q_1+q_2\equiv k]{(p_1+p_2)^2=s} &= i\frac{e^2}{s}\bar{v}^s(p_1)\gamma^\mu u^r(p_2)\epsilon_{\mu\nu\alpha\beta}n^\nu(q_2)q_1^\alpha k^\beta f_{\omega\pi^0}(s). \end{aligned} \tag{B.16}$$

Squaring this and averaging/summing over spin/polarization states, we get

$$\begin{aligned} \overline{|\mathcal{M}_3|^2} &= \frac{1}{4}\sum\left(\frac{e^2}{s}\right)^2(\bar{v}^s(p_1)\gamma^\mu u^r(p_2))^*\,\epsilon_{\mu\nu\alpha\beta}(n^\nu(q_2))^* q_1^\alpha k^\beta\times \\ &\qquad\times(\bar{v}^s(p_1)\gamma^\sigma u^r(p_2))\,\epsilon_{\sigma\rho\lambda\kappa}(n^\rho(q_2))q_1^\lambda k^\kappa|f_{\omega\pi^0}(s)|^2 \\ &= \frac{1}{4}\sum\left(\frac{e^2}{s}\right)^2(\bar{u}^r(p_1)\gamma^\mu v^s(p_2)\bar{v}^s(p_1)\gamma^\sigma u^r(p_2))\,\epsilon_{\mu\nu\alpha\beta}\epsilon_{\sigma\rho\lambda\kappa}\times \\ &\qquad\times(n^\nu(q_2))^*(n^\rho(q_2))q_1^\alpha q_1^\lambda k^\beta k^\kappa|f_{\omega\pi^0}(s)|^2. \end{aligned} \tag{B.17}$$

After the summation, fermion parts transform into a trace as in (B.5) and the vector meson polarization sum will yield the metric tensor (see [Schneider 2012] for details). Finally,

$$\begin{aligned} \overline{|\mathcal{M}_3|^2} &= -\left(\frac{e^2}{s}\right)^2\frac{1}{4}\mathrm{tr}\left(\gamma^\mu\left(\not{p}_1-m_e\right)\gamma^\sigma\left(\not{p}_2+m_e\right)\right)\left(\epsilon_{\mu\nu\alpha\beta}\epsilon_\sigma{}^\nu{}_{\lambda\kappa}q_1^\alpha q_1^\lambda k^\beta k^\kappa\right)|f_{\omega\pi^0}(s)|^2 \\ \xrightarrow{(B.6)} &= \left(\frac{e^2}{s}\right)^2\frac{1}{2}\Big(\left(k^2g^{\mu\sigma}-k^\mu k^\sigma\right)+(l^\mu l^\sigma)\Big)\left(\epsilon_{\mu\nu\alpha\beta}\epsilon_\sigma{}^\nu{}_{\lambda\kappa}q_1^\alpha q_1^\lambda k^\beta k^\kappa\right)|f_{\omega\pi^0}(s)|^2 \\ &= \left(\frac{e^2}{s}\right)^2\frac{1}{2}\Bigg(k^2\epsilon_{\mu\nu\alpha\beta}\epsilon^{\mu\nu}{}_{\lambda\kappa}q_1^\alpha q_1^\lambda k^\beta k^\kappa+\epsilon_{\mu\nu\alpha\beta}\epsilon_\sigma{}^\nu{}_{\lambda\kappa}l^\mu l^\sigma q_1^\alpha q_1^\lambda k^\beta k^\kappa\Bigg)|f_{\omega\pi^0}(s)|^2. \end{aligned} \tag{B.18}$$

To proceed, recall

$$\begin{aligned} &\epsilon_{\mu\nu\alpha\beta}\epsilon^{\mu\nu}{}_{\lambda\kappa} = 2(g_{\alpha\kappa}g_{\beta\lambda}-g_{\alpha\lambda}g_{\beta\kappa}), \\ &\epsilon_{\mu\nu\alpha\beta}\epsilon_\sigma{}^\nu{}_{\lambda\kappa} = -g_{\alpha\sigma}g_{\beta\lambda}g_{\kappa\mu}+g_{\alpha\lambda}g_{\beta\sigma}g_{\kappa\mu}+g_{\alpha\sigma}g_{\beta\kappa}g_{\lambda\mu}-g_{\alpha\kappa}g_{\beta\sigma}g_{\lambda\mu}-g_{\alpha\lambda}g_{\beta\kappa}g_{\mu\sigma}+g_{\alpha\kappa}g_{\beta\lambda}g_{\mu\sigma}. \end{aligned} \tag{B.19}$$

So,

$$\begin{aligned} k^2\epsilon_{\mu\nu\alpha\beta}\epsilon^{\mu\nu}{}_{\lambda\kappa}q_1^\alpha q_1^\lambda k^\beta k^\kappa &= 2k^2\left((q_1\cdot k)^2-q_1^2k^2\right) \\ &= \frac{s}{2}\lambda(s,m_\pi^2,m_\omega^2), \\ \epsilon_{\mu\nu\alpha\beta}\epsilon_\sigma{}^\nu{}_{\lambda\kappa}l^\mu l^\sigma q_1^\alpha q_1^\lambda k^\beta k^\kappa &= (q_1\cdot l)^2k^2+(q_1\cdot k)^2l^2-q_1^2k^2l^2 \\ &= \frac{1}{4s}\lambda(s,m_\pi^2,m_\omega^2)\lambda(s,m_e,m_e)\left(\cos^2(\theta_s)-1\right). \end{aligned} \tag{B.20}$$

Using this,

$$\overline{|\mathcal{M}_3|^2} = \left(\frac{e^2}{s}\right)^2\frac{s}{4}\lambda(s,m_\pi^2,m_\omega^2)\left(1-\frac{\lambda(s,m_e,m_e)}{2s^2}\left(1-\cos^2(\theta_s)\right)\right)|f_{\omega\pi^0}(s)|^2. \tag{B.21}$$

Integrating $\overline{|\mathcal{M}_3|^2}$ over the solid angle, one obtains:

$$\int\overline{|\mathcal{M}_3|^2}d\Omega = \frac{2\pi e^4}{4s}\lambda(s,m_\pi^2,m_\omega^2)\int_{-1}^{+1}\left(1-\frac{\lambda(s,m_e,m_e)}{2s^2}\left(1-\cos^2(\theta_s)\right)\right)|f_{\omega\pi^0}(s)|^2d\cos(\theta_s)$$

$$
\begin{aligned}
&= \frac{\pi e^4}{s}\lambda(s, m_\pi^2, m_\omega^2)\frac{1}{2}\left(2 - \frac{\lambda(s, m_e, m_e)}{2s^2}\left(2 - \frac{2}{3}\right)\right)|f_{\omega\pi^0}(s)|^2 \\
&= \frac{\pi e^4}{s}\lambda(s, m_\pi^2, m_\omega^2)\underbrace{\left(1 - \frac{1}{3}\frac{\lambda(s, m_e, m_e)}{s^2}\right)}_{=2/3 \text{ for } m_e \ll s}|f_{\omega\pi^0}(s)|^2. \qquad \text{(B.22)}
\end{aligned}
$$

Defining as before,

$$
[\xi_3(s)]^2 = \frac{1}{3}\frac{\lambda(s, m_\pi^2, m_\omega^2)}{s}, \qquad \text{(B.23)}
$$

we have

$$
\int \overline{|\mathcal{M}_3|^2} d\Omega = (4\pi)e^2[\xi_{e^+e^-}(s)]^2 \frac{1}{s^2} e^2 [\xi_3(s)]^2 \frac{s}{2} |f_{\omega\pi^0}(s)|^2. \qquad \text{(B.24)}
$$

Using (2.14),

$$
\begin{aligned}
\sigma_{e^+e^-\to\pi^0\omega} &= \frac{1}{64\pi^2}\frac{\lambda^{1/2}(s, m_\pi^2, m_\omega^2)}{\lambda^{1/2}(s, m_e^2, m_e^2)}\frac{1}{s}\int \overline{|\mathcal{M}_3|^2} d\Omega \\
&= \frac{\pi e^4}{64\pi^2 s^2}\frac{\lambda^{3/2}(s, m_\pi^2, m_\omega^2)}{\lambda^{1/2}(s, m_e^2, m_e^2)}\left(1 - \frac{1}{3}\frac{\lambda(s, m_e, m_e)}{s^2}\right)|f_{\omega\pi^0}(s)|^2 \\
\xrightarrow[\alpha = e^2/4\pi]{m_e^2 \ll s} &= \frac{16\pi^3\alpha^2}{64\pi^2 s^2}\frac{\lambda^{3/2}(s, m_\pi^2, m_\omega^2)}{s}\left(1 - \frac{1}{3}\right)|f_{\omega\pi^0}(s)|^2 \\
&= \frac{\pi\alpha^2}{3}\frac{\lambda^{3/2}(s, m_\pi^2, m_\omega^2)}{s^4}\underbrace{\frac{s}{2}|f_{\omega\pi^0}(s)|^2}_{|F_3(s)|^2}. \qquad \text{(B.25)}
\end{aligned}
$$

Note that (B.25) has almost the same form as (B.13). They become exactly identical if one absorbs the extra factor of $s/2$ in the definition of the form factor, i.e. $F_3(s) \equiv \sqrt{s/2} f_{\omega\pi^0}(s)$.

C The two-potential model

C.1 Self-energy and resonance potential

For the calculation of the discontinuity of the self-energy Σ_k, we need to first consider the discontinuities of its constituent parts: centrifugal barrier factor, channel propagator and vertex. Centrifugal barrier factors are basically powers of momenta and have no discontinuity. The discontinuity of the propagator can be derived from the Lippmann-Schwinger equation:

$$
\begin{aligned}
T &= V + VGT, \\
\mathrm{disc}\,[T] &= T - T^* \\
&= VGT - VG^*T^* \\
&= VGT - VGT^* + VGT^* - VG^*T^* \\
&= VG\ \mathrm{disc}\,[T] + V\ \mathrm{disc}\,[G]\,T^* \\
\xrightarrow{(A.5)} &= VG\ T2i\sigma T^* + V\ \mathrm{disc}\,[G]\,T^*, \\
\xrightarrow{(A.5)} \mathrm{disc}\,[T] &= T2i\sigma T^*, \\
\implies \mathrm{disc}\,[G] &= 2i\sigma.
\end{aligned}
\tag{C.1}
$$

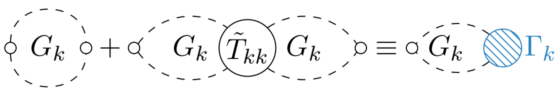

$$
\implies \quad G_k + G_k\tilde{T}_{kk}G_k \equiv G_k\xi_k\Gamma_{k,\mathrm{out}}. \tag{C.2}
$$

Vertices are defined so that they include elastic rescattering (C.2). We have already calculated the discontinuity due to elastic scattering in Appendix A.2. This will be similar to the one for the form factor (A.13):

$$
\mathrm{disc}\,[\Gamma] = 2i\sigma\tilde{T}^*\Gamma. \tag{C.3}
$$

Finally, the discontinuity of Σ_k can be derived as follows:

$$
\begin{aligned}
\mathrm{disc}\,[\Sigma_k] &= \mathrm{disc}\,[\xi_k G_k \Gamma_k \xi_k] \\
&= \xi_k^2\,(\mathrm{disc}\,[G_k]\,\Gamma_k + G_k^*\mathrm{disc}\,[\Gamma_k]) \\
\xrightarrow{(C.1,C.3)} &= \xi_k^2\left(2i\sigma_k\Gamma_k + 2i\sigma_k G_k^*\tilde{T}_{kk}^*\Gamma_k\right) \\
&= 2i\sigma_k\xi_k^2\left(1 + G_k^*\tilde{T}_{kk}^*\right)\Gamma_k \\
&= 2i\sigma_k\xi_k^2|\Gamma_k|^2.
\end{aligned}
\tag{C.4}
$$

This allows us to write the integral solution for Σ_k as (2.47).

The resonance t-matrix is defined as

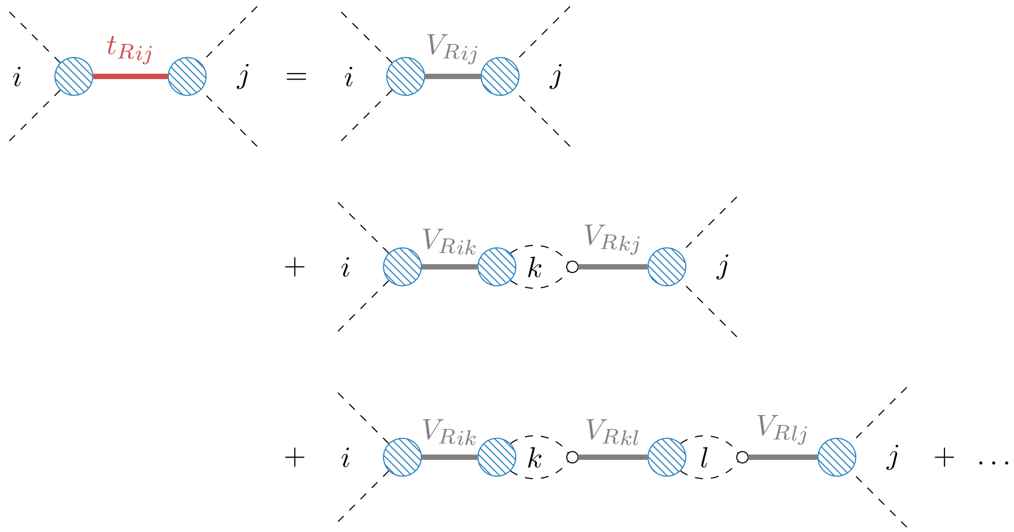

(C.5)

Note that wherever applicable, elastic rescattering is taken care of by the vertices (see (C.2)). Finally,

$$
\begin{aligned}
(\xi_i\Gamma_i)t_{Rij}(\xi_j\Gamma_j) &= (\xi_i\Gamma_i)V_{Rij}(\xi_j\Gamma_j) \\
&+ (\xi_i\Gamma_i)V_{Rik}(\xi_k G_k \Gamma_k \xi_k)V_{Rkj}(\xi_j\Gamma_j) \\
&+ (\xi_i\Gamma_i)V_{Rik}\underbrace{(\xi_k G_k \Gamma_k \xi_k)}_{\Sigma_k}V_{Rkl}(\xi_l G_l \Gamma_l \xi_l)V_{Rlj}(\xi_j\Gamma_j) + \dots \\
&= (\xi_i\Gamma_i)\left[\sum_{n=0}^{\infty} V_R\Sigma\right]_{ik} V_{Rkj}(\xi_j\Gamma_j) \\
&= (\xi_i\Gamma_i)\left[\mathbb{1}_C - V_R\Sigma\right]^{-1}_{ik} V_{Rkj}(\xi_j\Gamma_j) \\
&= (\xi_i\Gamma_i)\left[[\mathbb{1}_C - V_R\Sigma]^{-1}V_R\right]_{ij}(\xi_j\Gamma_j),
\end{aligned}
\tag{C.6}
$$

where it should be clear, that

$$
[V_R\Sigma]_{ij} = V_{Rij}\Sigma_j. \tag{C.7}
$$

In the end,

$$
t_R = [\mathbb{1}_C - V_R\Sigma]^{-1}V_R. \tag{C.8}
$$

C.2 Form factor

The expression for the form factor using the two-potential formalism can be derived as follows:

$$
\xi_i F_i = \xi_i M_i + T_{ij} G_j \xi_j M_j, \tag{C.9}
$$

$$
\begin{aligned}
F_i &= M_i + T_{ij} G_j (\xi_j/\xi_i) M_j \\
&= \left(\delta_{ij} + \tilde{T}_{ij} G_j (\xi_j/\xi_i) + T_{Rij} G_j (\xi_j/\xi_i)\right) M_j \\
&= \left(\delta_{ij}(1 + \tilde{T}_{ii} G_i) + T_{Rij} G_j (\xi_j/\xi_i)\right) M_j \\
&= \left(\delta_{ij}\Gamma_{\mathrm{out},i} + T_{Rij} G_j (\xi_j/\xi_i)\right) M_j
\end{aligned}
$$

$$
\begin{aligned}
&= \left(\delta_{ij}\Gamma_{\mathrm{out},i} + \xi_i\Gamma_{\mathrm{out},i}t_{Rij}\xi_j\Gamma^\dagger_{\mathrm{in},j}G_j(\xi_j/\xi_i)\right)M_j \\
&= \Gamma_{\mathrm{out},i}\left(\delta_{ij} + t_{Rij}\xi_j^2\Gamma^\dagger_{\mathrm{in},j}G_j\right)M_j \\
&= \Gamma_{\mathrm{out},i}\left(\delta_{ij} + t_{Rij}\Sigma_j\right)M_j.
\end{aligned}
\tag{C.10}
$$

Note that

$$
\begin{aligned}
&t_R = [\mathbb{1}_C - V_R\Sigma]^{-1}V_R \\
\implies\; &t_R\Sigma = [\mathbb{1}_C - V_R\Sigma]^{-1}V_R\Sigma = -\mathbb{1}_C + [\mathbb{1}_C - V_R\Sigma]^{-1}.
\end{aligned}
\tag{C.11}
$$

So,

$$
\begin{aligned}
F_i &= \Gamma_{\mathrm{out},i}\left(\delta_{ij} + (-\delta_{ij}) + [\mathbb{1}_C - V_R\Sigma]^{-1}_{ij}\right)M_j \\
&= \Gamma_{\mathrm{out},i}[\mathbb{1}_C - V_R\Sigma]^{-1}_{ij}M_j.
\end{aligned}
\tag{C.12}
$$

The discontinuity of the above expression can be calculated as follows:

$$
\begin{aligned}
\mathrm{disc}\,[F_i] &= \mathrm{disc}\,[\Gamma_{\mathrm{out},i}]\,[\mathbb{1}_C - V_R\Sigma]^{-1}M + \Gamma^*_{\mathrm{out},i}\mathrm{disc}\left[[\mathbb{1}_C - V_R\Sigma]^{-1}\right]M \\
&= \underbrace{\mathrm{disc}\,[\Gamma_{\mathrm{out},i}]}_{2i\tilde{T}_{ii}\sigma_i\Gamma_{\mathrm{out},i}}[\mathbb{1}_C - V_R\Sigma]^{-1}M + \Gamma^*_{\mathrm{out},i}[\mathbb{1}_C - V_R\Sigma]^{-1}V_R\,\underbrace{\mathrm{disc}\,[\Sigma_k]}_{2i\sigma_k\xi_k^2|\Gamma_k|^2}\,[\mathbb{1}_C - V_R\Sigma]^{-1}M \\
&= 2i\underbrace{\left(\tilde{T}^*_{ii}\delta_{ik} + \xi_i\Gamma^*_{\mathrm{out},i}t_{Rik}\Gamma^*_{\mathrm{out},k}\xi_k\right)}_{T^*_{ik}}\sigma_k(\xi_k/\xi_i)\,\underbrace{\Gamma_{\mathrm{out},k}[\mathbb{1}_C - V_R\Sigma]^{-1}_{kj}M_j}_{F_k} \\
&= 2iT^*_{ik}\sigma_k(\xi_k/\xi_i)F_k.
\end{aligned}
\tag{C.13}
$$

C.2.1 Form factor at $s = 0$

Within the resonance model, where photon mixing is allowed, V_R is given by (2.57). This means, that

$$
\begin{aligned}
F_i(0) &= \underbrace{\Gamma_{\mathrm{out},i}(0)}_{1}\left[\mathbb{1}_C - \left(-e^2\frac{cc^T}{s}\Sigma(s)\right)\Bigg|_{s=0}\right]^{-1}_{ik}c_k \\
&= \left[\mathbb{1}_C - \left(-e^2\frac{cc^T}{s}\frac{s}{\pi}\int_{s_{\mathrm{thr},i}}^\infty\frac{ds'}{s'}\frac{\sigma(s')\xi^2(s')|\Gamma(s')|^2}{s'-s}\right)\Bigg|_{s=0}\right]^{-1}_{ik}c_k \\
&= \left[\mathbb{1}_C - \left(-e^2cc^T\underbrace{\frac{1}{\pi}\int_{s_{\mathrm{thr},i}}^\infty\frac{ds'\sigma(s')\xi^2(s')|\Gamma(s')|^2}{(s')^2}}_{\mathcal{B}}\right)\right]^{-1}_{ik}c_k \\
&= \left[\mathbb{1}_C - \left(-e^2cc^T\mathcal{B}\right)\right]^{-1}_{ik}c_k \\
&= \left[\mathbb{1}_C + \left(-e^2cc^T\mathcal{B}\right) + \left(-e^2cc^T\mathcal{B}\right)^2 + \dots\right]_{ik}c_k \\
&= \left[\delta_{ik} + \left(-e^2\right)c_ic_k\mathcal{B}_k + \left(-e^2\right)^2c_ic_l\mathcal{B}_lc_lc_k\mathcal{B}_k + \dots\right]c_k \\
&= c_i\left[1 + \left(-e^2\right)c_k^2\mathcal{B}_k + \left(-e^2\right)^2c_l^2\mathcal{B}_lc_k^2\mathcal{B}_k + \dots\right] \\
&= c_i\left[1 - \left(-e^2\right)c_k^2\mathcal{B}_k\right]^{-1}
\end{aligned}
$$

$$= c_i \left[1 - \underbrace{\left(-e^2\right) c_k^2 \frac{1}{\pi} \int_{s_{\mathrm{thr},i}}^{\infty} \frac{ds' \sigma_k(s') \xi_k^2(s') |\Gamma_k(s')|^2}{(s')^2}}_{\delta} \right]^{-1} . \tag{C.14}$$

Therefore, to obtain $F_i(0) = c_i$, one needs to redefine the normalization constants:

$$c_i \to c_i[1 - \delta]. \tag{C.15}$$

References

Abe, M., Bae, S., Beer, G., Bunce, G., Choi, H., Choi, S., Chung, M., da Silva, W., Eidelman, S., Finger, M., et al. (2019). A new approach for measuring the muon anomalous magnetic moment and electric dipole moment.

Achasov, N. N. and Kozhevnikov, A. A. (2013). Pion form factor and reactions $e^+e^- \to \omega\pi^0$ and $e^+e^- \to \pi^+\pi^-\pi^+\pi^-$ at energies up to 2–3 GeV in the many-channel approach. *Physical Review D*, 88(9).

Aoyama, T., Asmussen, N., Benayoun, M., Bijnens, J., Blum, T., Bruno, M., Caprini, I., Carloni Calame, C., Cè, M., Colangelo, G., et al. (2020). The anomalous magnetic moment of the muon in the Standard Model. *Physics Reports*, 887:1–166.

BaBaR (2012). Precise measurement of the $e^+e^- \to \pi^+\pi^-(\gamma)$ cross section with the initial-state radiation method at BABAR. *Physical Review D*, 86(3).

BaBaR (2017). Measurement of the $e^+e^- \to \pi^+\pi^-\pi^0\pi^0$ cross section using initial-state radiation at BABAR. *Physical Review D*, 96(9).

BELLE (2008). High-statistics study of the $\tau^- \to \pi^-\pi^0\nu_\tau$ decay. *Phys. Rev. D*, 78:072006.

BNL (2006). Final report of the E821 muon anomalous magnetic moment measurement at BNL. *Physical Review D*, 73(7).

Bondar, A., Eidelman, S., Milstein, A., and Root, N. (1999). On the role of the $a_1(1260)$ meson in $\tau \to 4\pi\nu_\tau$ decay. *Physics Letters B*, 466(2-4):403–407.

Caprini, I., Colangelo, G., and Leutwyler, H. (2012). Regge analysis of the $\pi\pi$ scattering amplitude. *The European Physical Journal C*, 72(2).

CMD-2 (1999). $a_1(1260)\pi$ dominance in the process $e^+e^- \to 4\pi$ at energies 1.05-GeV - 1.38-GeV. *Phys. Lett. B*, 466:392–402.

CMD-2 (2003). Study of the process $e^+e^- \to \omega\pi^0 \to \pi^0\pi^0\gamma$ in c.m. energy range 920–1380 MeV at CMD-2. *Physics Letters B*, 562(3-4):173–181.

CMD-2 (2005). Measurement of the pion form-factor in the range 1.04-GeV to 1.38-GeV with the CMD-2 detector. *JETP Lett.*, 82:743–747.

CMD-2 (2007). High-statistics measurement of the pion form factor in the -meson energy range with the cmd-2 detector. *Physics Letters B*, 648(1):28–38.

Colangelo, G., Gasser, J., and Leutwyler, H. (2001). $\pi\pi$ scattering. *Nuclear Physics B*, 603(1-2):125–179.

Colangelo, G., Hoferichter, M., Procura, M., and Stoffer, P. (2017). Dispersion relation for hadronic light-by-light scattering: two-pion contributions. *Journal of High Energy Physics*, 2017(4).

Colangelo, G., Hoferichter, M., and Stoffer, P. (2019). Two-pion contribution to hadronic vacuum polarization. *Journal of High Energy Physics*, 2019(2).

Dalitz, R. H. (1961). On the strong interactions of the strange particles. *Rev. Mod. Phys.*, 33:471–492.

Dembinski, H., Ongmongkolkul, P., et al. (2020). scikit-hep/iminuit.

Eden, R. J., Landshoff, P. V., Olive, D. I., and Polkinghorne, J. C. (1966). *The analytic S-matrix.* Cambridge Univ. Press, Cambridge.

Eidelman, S. and Łukaszuk, L. (2004). Pion form factor phase, $\pi\pi$ elasticity and new e^+e^- data. *Physics Letters B*, 582(1-2):27–31.

FNAL (2021). Measurement of the positive muon anomalous magnetic moment to 0.46 ppm. *Phys. Rev. Lett.*, 126:141801.

García-Martín, R., Kamiński, R., Peláez, J. R., Ruiz de Elvira, J., and Ynduráin, F. J. (2011). Pion-pion scattering amplitude. IV. improved analysis with once subtracted Roy-like equations up to 1100 MeV. *Physical Review D*, 83(7).

Gounaris, G. J. and Sakurai, J. J. (1968). Finite-width corrections to the vector-meson-dominance prediction for $\rho \to e^+e^-$. *Phys. Rev. Lett.*, 21:244–247.

Hanhart, C. (2012). A new parameterization for the pion vector form factor. *Physics Letters B*, 715(1-3):170–177.

Hatlo, M., James, F., Mato, P., Moneta, L., Winkler, M., and Zsenei, A. (2005). Developments of mathematical software libraries for the LHC experiments. *IEEE Trans. Nucl. Sci.*, 52:2818–2822.

James, F. and Roos, M. (1975). Minuit: A System for Function Minimization and Analysis of the Parameter Errors and Correlations. *Comput. Phys. Commun.*, 10:343–367.

Jegerlehner, F. and Szafron, R. (2011). $\rho^0 - \gamma$ mixing in the neutral channel pion form factor F_π^e and its role in comparing e^+e^- with τ spectral functions. *Eur. Phys. J. C*, 71:1632.

KLOE (2005). Measurement of $\sigma(e^+e^- \to \pi^+\pi^-\gamma)$ and extraction of $\sigma(e^+e^- \to \pi^+\pi^-)$ below 1-GeV with the KLOE detector. *Phys. Lett. B*, 606:12–24.

MAMI (2017). Measurement of the $\omega \to \pi^0e^+e^-$ and $\eta \to e^+e^-\gamma$ Dalitz decays with the A2 setup at the Mainz Microtron. *Physical Review C*, 95(3).

NA60 (2009). Study of the electromagnetic transition form-factors in $\eta \to \mu^+\mu^-\gamma$ and $\omega \to \mu^+\mu^-\pi^0$ decays with NA60. *Physics Letters B*, 677(5):260–266.

NA60 (2016). Precision study of the $\eta \to \mu^+\mu^-\gamma$ and $\omega \to \mu^+\mu^-\pi^0$ electromagnetic transition form-factors and of the $\rho \to \mu^+\mu^-$ line shape in NA60. *Physics Letters B*, 757:437–444.

Nakano, K. (1982). Two-potential formalisms and the Coulomb-nuclear interference. *Phys. Rev. C*, 26:1123–1131.

Omnès, R. (1958). On the Solution of certain singular integral equations of quantum field theory. *Nuovo Cim.*, 8:316–326.

PDG (2020). Review of Particle Physics. *Progress of Theoretical and Experimental Physics*, 2020(8). 083C01.

Ropertz, S., Hanhart, C., and Kubis, B. (2018). A new parametrization for the scalar pion form factors. *The European Physical Journal C*, 78(12).

Roy, S. (1971). Exact integral equation for pion-pion scattering involving only physical region partial waves. *Physics Letters B*, 36(4):353–356.

Schneider, S. P. (2012). *Analysis tools for precision studies of hadronic three-body decays and transition form factors.* PhD thesis, Bonn U., HISKP.

Schneider, S. P., Kubis, B., and Niecknig, F. (2012). $\omega \to \pi^0\gamma^*$ and $\phi \to \pi^0\gamma^*$ transition form factors in dispersion theory. *Phys. Rev. D*, 86:054013.

SND (2000). The process $e^+e^- \to \omega\pi^0 \to \pi^0\pi^0\gamma$ up to 1.4 GeV. *Physics Letters B*, 486(1-2):29–34.

SND (2005). Study of the process $e^+e^- \to \pi^+\pi^-$ in the energy region $400 < \sqrt{s} < 1000$ MeV. *Journal of Experimental and Theoretical Physics*, 101(6):1053–1070.

SND (2016). Updated measurement of the $e^+e^- \to \omega\pi^0 \to \pi^0\pi^0\gamma$ cross section with the SND detector. *Physical Review D*, 94(11).

von Detten, L., Noël, F., Hanhart, C., Hoferichter, M., and Kubis, B. (2021). On the scalar πK form factor beyond the elastic region. *The European Physical Journal C*, 81(5).

Watson, K. M. (1954). Some general relations between the photoproduction and scattering of π mesons. *Phys. Rev.*, 95:228–236.